

Discovery of 1*H*-Pyrazol-3(2*H*)-ones as Potent and Selective Inhibitors of Protein Kinase R-like Endoplasmic Reticulum Kinase (PERK)

Adrian L. Smith,^{*,†} Kristin L. Andrews,[‡] Holger Beckmann,[¶] Steven F. Bellon,[⊥] Pedro J. Beltran,[§] Shon Booker,[†] Hao Chen,[#] Young-Ah Chung,[§] Noel D. D'Angelo,[†] Jennifer Dao,[‡] Kenneth R. Dellamaggiore,[§] Peter Jaeckel,[¶] Richard Kendall,[§] Katja Labitzke,[¶] Alexander M. Long,[⊥] Silvia Materna-Reichelt,[¶] Petia Mitchell,[§] Mark H. Norman,[†] David Powers,[‡] Mark Rose,^{||} Paul L. Shaffer,[⊥] Michelle M. Wu,[§] and J. Russell Lipford^{*,§}

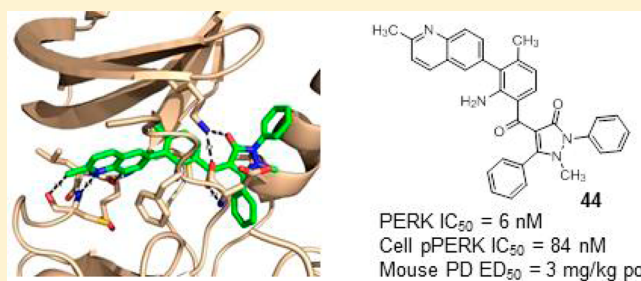
Departments of [†]Medicinal Chemistry, [‡]Molecular Structure and Characterization, [§]Oncology Research, and ^{||}Pharmacokinetics and Drug Metabolism, Amgen Inc., One Amgen Center Drive, Thousand Oaks, California 91320-1799, United States

Departments of [⊥]Molecular Structure and Characterization and [#]Protein Technologies, Amgen Inc., 360 Binney Street, Cambridge, Massachusetts 02142, United States

[¶]Amgen Research GmbH, Josef-Engert-Straße 11, D-93053 Regensburg, Germany

S Supporting Information

ABSTRACT: The structure-based design and optimization of a novel series of selective PERK inhibitors are described resulting in the identification of **44** as a potent, highly selective, and orally active tool compound suitable for PERK pathway biology exploration both in vitro and in vivo.

**■ INTRODUCTION**

The unfolded protein response (UPR) is an evolutionarily conserved mechanism in mammals by which cells respond to endoplasmic reticulum (ER) stress.¹ Cellular ER stress is characterized by an accumulation of misfolded proteins in the ER lumen resulting from an inability of the cell to adequately process protein production in the ER, for example, under nutrient deprivation conditions (hypoxia, glucose starvation) or where a high secretory load exists. There are three sensors of misfolded proteins that are known to mediate the UPR through complementary pathways: protein kinase R-like endoplasmic reticulum kinase (PERK), inositol-requiring enzyme 1 (IRE1), and activating transcription factor 6 (ATF6).² PERK, IRE1, and ATF6 are all located in the ER membrane and sense misfolded proteins in the ER lumen through the molecular chaperone BiP/Grp78 and/or direct binding of unfolded proteins to the sensor domains.³ The UPR serves as a mechanism for cellular survival whereby cells are able to adapt to cope with ER stress, but under extreme stress the UPR switches the cellular machinery toward apoptosis.^{4–6} The UPR is known to be active in highly secretory tissues such as the pancreas,⁷ but tumors are also thought to utilize the UPR for survival under stressed conditions such as nutrient deprivation or chemotherapeutic insult.⁸ This suggests that modulators of the UPR

may be useful for the treatment of cancer^{9–11} either as a sole agent or in combination with other anticancer treatments, thus spurring recent interest in the identification of UPR pathway inhibitors.

PERK is an ER transmembrane protein with a stress-sensing domain inside the ER lumen and a cytosolic kinase domain.¹⁰ Upon sensing misfolded proteins, PERK is activated by autophosphorylation and oligomerization through release of BiP/Grp78 from the stress-sensing domain. Activated PERK phosphorylates and activates its downstream substrate, eukaryotic initiation factor 2 α (eIF2 α), which inhibits the ribosome translation initiation complex in order to attenuate protein synthesis. This serves to prevent exacerbation of ER stress by preventing the accumulation of additional misfolded proteins. Although it inhibits general protein synthesis, activated eIF2 α causes the translation of specific mRNAs involved in restoring ER homeostasis including activating transcription factor 4 (ATF4). ATF4 mediates the transcription of certain UPR target genes including those for the endoplasmic-reticulum-associated protein degradation (ERAD) pathway proteins which target misfolded proteins

Received: November 11, 2014

for ubiquitination and degradation by the proteasome. ATF4 also causes the expression of the transcription factor C/EBP homologous protein (CHoP), which sensitizes cells to ER stress-mediated apoptosis, providing a pathway for regulated removal of severely stressed cells by the organism. There were no known selective PERK inhibitors at the outset of our work exploring the UPR, and this prompted us to initiate a search for tool compounds to validate PERK as an oncology target. The first potent and selective PERK inhibitors have since been disclosed by Axten^{12,13} including GSK2606414, its fluorinated analog **1**, and the analog GSK2656157 which was optimized for preclinical evaluation (Figure 1). Our research leading to the

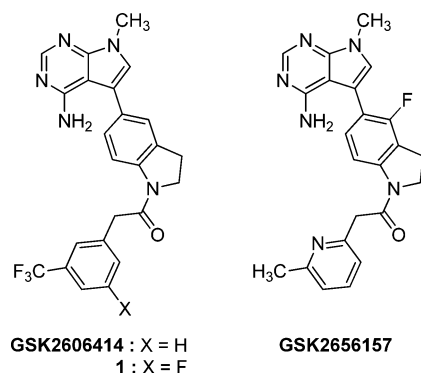


Figure 1. Structures of previously disclosed PERK inhibitors.

identification of a novel series of potent, orally active PERK inhibitors with high selectivity over other kinases is described in this article. The use of these inhibitors for exploration of PERK pathway biology as well as PERK target validation *in vivo* will be described elsewhere.

RESULTS AND DISCUSSION

Chemistry. The screening hit **7**, originally prepared as part of an earlier exploration of B-Raf inhibitor structure–activity relationships (SARs),¹⁴ was readily prepared in three steps (an amide coupling, a nitro reduction, and a Suzuki–Miyaura coupling¹⁵) as shown in Scheme 1. The screening hits **10a,b** originated from a prior *c*-MET inhibitor program and were synthesized from previously reported intermediates^{16,17} using more forcing amide coupling conditions (Scheme 2).

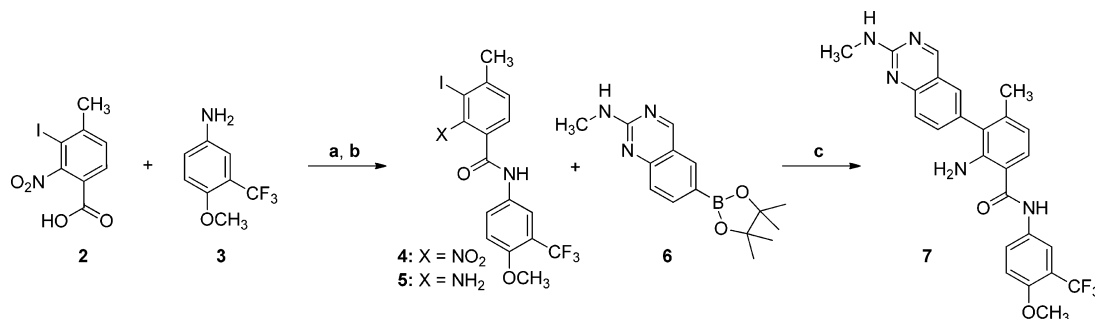
Target molecules were synthesized from the key intermediates shown in Schemes 3–5. 4-Benzoyl-1*H*-pyrazol-3(2*H*)-one intermediates **13a–d** (Scheme 3) were prepared

by selective C-acylation of the 1*H*-pyrazol-3(2*H*)-one **12**¹⁸ and subsequent N-methylation. Reduction of the nitro intermediates **13a,c** to the corresponding amino intermediates **14a,c** was conveniently accomplished with iron in acetic acid. 6-Quinazolinylylboronate ester intermediates **19a–c** were prepared as shown in Scheme 4; intermediates **6**¹⁴ and **17a**¹⁹ have been previously described, and **18c** was acquired from commercial sources. The 2-methylaminoquinazoline **18b** was most readily accessed via a three-step process from fluoroaldehyde **15** involving initial formation of the 2-aminoquinazoline **16**, chloro-deamination using a modification of the Sandmeyer reaction (to give **17b**), followed by amination with methylamine. More direct routes from **15** to **18b**, such as reaction of **15** with methylguanidine or methylation of **16**, were problematic because of regiochemistry issues. The 6-bromoquinazolines **18a–c** were readily converted to the corresponding boronate esters **19a–c**.²⁰ The corresponding 2-methyl-6-quinolylboronate ester **20** is commercially available. Benzothiazolylboronate ester intermediates were accessed as outlined in Scheme 5. The benzothiazole derivatives **21–24** and **28c** were obtained from commercial sources, and the fluorinated derivatives **28a,b** were accessed using variations on a procedure involving N-acylation of the 2-aminothiophenols **25** and **26** followed by facile cyclization–dehydration under reductive conditions to form the benzothiazoles **28a,b**. The bromides **28a–c** were then converted to the corresponding boronate esters **29a–c**.

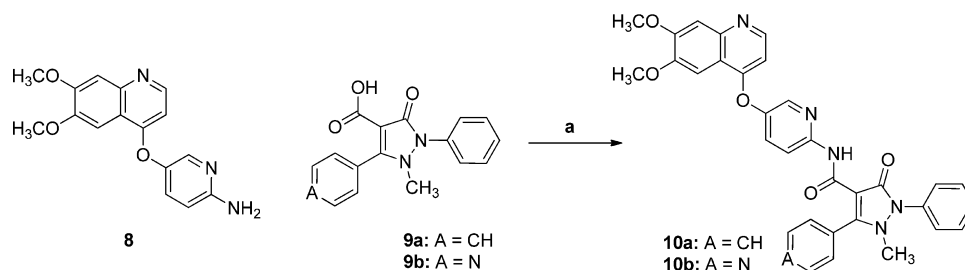
The final stages of the syntheses of the PERK inhibitors **30–44** are shown Scheme 6. Compounds **30–33**, **37–40**, and **42–44** were directly synthesized in one step from the appropriate benzoyl-1*H*-pyrazol-3(2*H*)-one intermediates **13b**, **13d**, **14a**, and **14c** using a Suzuki–Miyaura coupling with the corresponding boronate esters shown in Schemes 4 and 5. Compounds **34–36** and **41** were prepared in a generally less efficient overall two-step process by similarly coupling the 4-(2-nitrobenzoyl)-1*H*-pyrazol-3(2*H*)-one **13a** with the corresponding boronate ester, followed by reduction of the nitro group. The PERK inhibitor **52** was synthesized in a convergent manner using a Suzuki–Miyaura coupling to join the fragments **48** and **51** (Scheme 7).

Lead Optimization and SAR. No suitable medicinal chemistry leads for deriving a selective PERK inhibitor tool compound were known at the outset of this work, and so we performed a high-throughput screen of the Amgen sample collection looking for inhibitors of PERK kinase activity (phosphorylation of the downstream substrate eIF2 α). Hits were assessed for cellular activity in both a mechanism-based

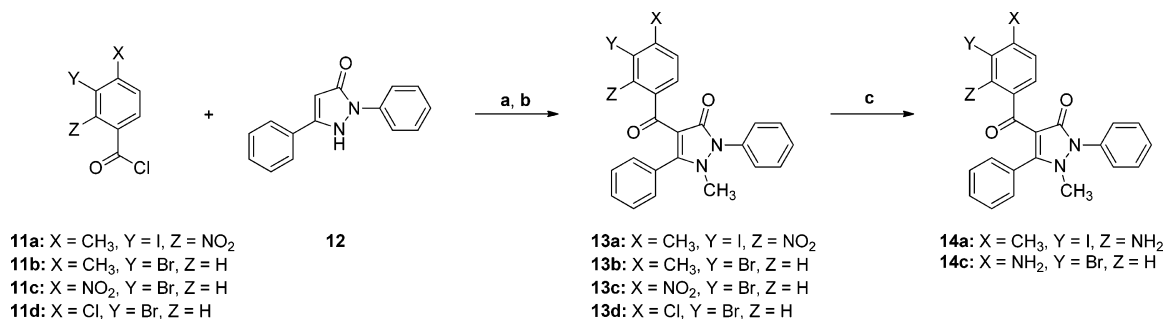
Scheme 1. Synthesis of Screening Hit **7**^a



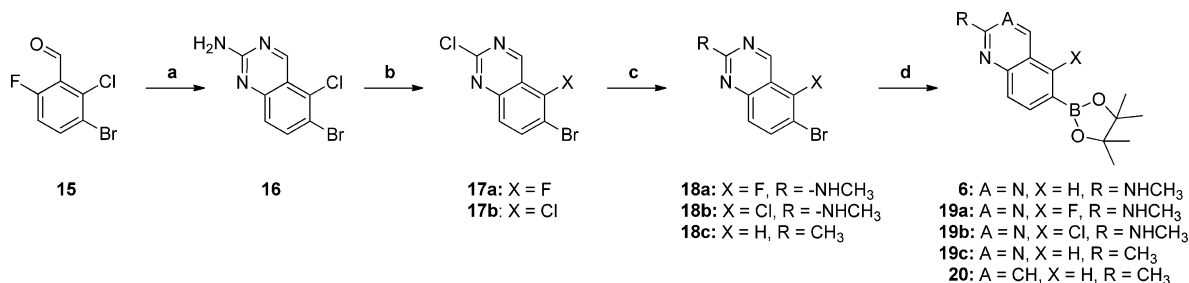
^aReagents and conditions: (a) TBTU, *i*-Pr₂NEt, DMF, rt, 2 h; (b) Fe, AcOH, EtOH, Δ , 3 h; (c) PdCl₂(PPh₃)₂ (cat.), Na₂CO₃·H₂O, DMF, H₂O, 150 °C (microwave), 15 min.

Scheme 2. Synthesis of Screening Hits 10a,b^a

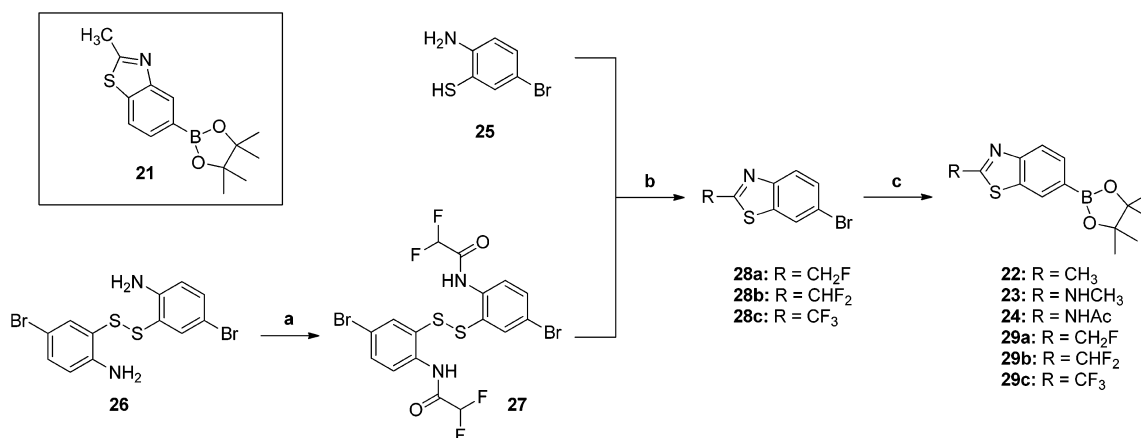
^aReagents and conditions: (a) HATU, Et₃N, DMF, 90 °C, 16 h.

Scheme 3. Synthesis of 4-Benzoyl-1*H*-pyrazol-3(2*H*)-one Intermediates 13a–d, 14a, and 14c^a

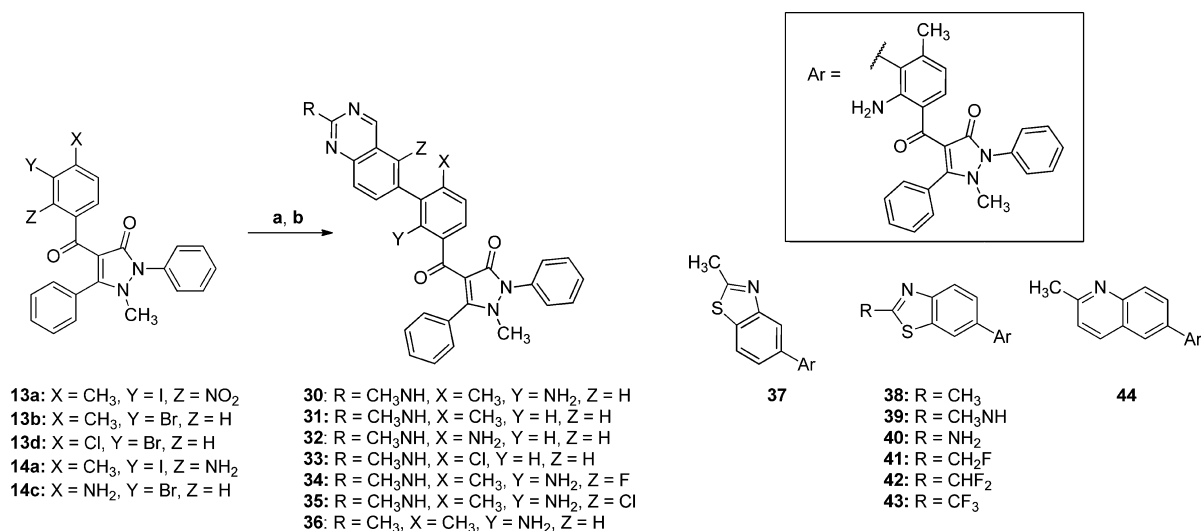
^aReagents and conditions: (a) Ca(OH)₂, 1,4-dioxane, 90 °C, 16 h; (b) methyl *p*-toluenesulfonate, 170 °C, 3 h; (c) Fe, AcOH, EtOH, Δ, 1.5 h.

Scheme 4. Synthesis of 6-Quinazolinyboronate Ester Intermediates 19a–c^a

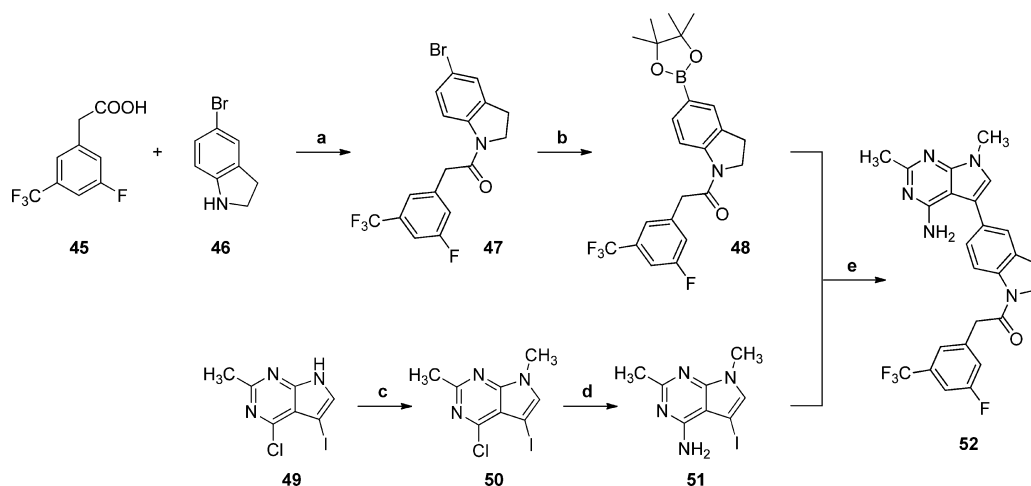
^aReagents and conditions: (a) guanidine carbonate, *i*-Pr₂NEt, NMP, 140 °C, 2 h; (b) *n*-Bu₄NCl, (CH₃)₃SiCl, *t*-BuONO, 0–50 °C, 1 h; (c) CH₃-NH₂, EtOH, 80 °C, 1 h; (d) bis(pinacolato)diboron, Pd(dppf)₂Cl₂·CH₂Cl₂, KOAc, 1,4-dioxane, Δ, 2.5 h.

Scheme 5. Synthesis of Benzothiazolylboronate Ester Intermediates 29a–c^a

^aReagents and conditions: (a) difluoroacetyl chloride, pyridine, CH₂Cl₂, rt, 2 h. (b) For 28a: fluoroacetic acid, 25, PPh₃, Et₃N, CCl₄, 95 °C, 1.5 h. For 28b: 27, dithiothreitol, DMF, rt, 16 h. (c) For 29a–c: bis(pinacolato)diboron, Pd(dppf)₂Cl₂·CH₂Cl₂, KOAc, 1,4-dioxane, 120 °C (microwave), 30 min.

Scheme 6. Synthesis of PERK Inhibitors 30–44^a

^aReagents and conditions: (a) boronate ester (Schemes 4 and 5). Method A: Pd(PPh₃)₄, K₃PO₄, toluene, MeOH, water, 100 °C, 8 h. Method B: bis(di-*tert*-butyl(4-dimethylaminophenyl)phosphine)dichloropalladium(II), Na₂CO₃, DMF, water, 110 °C, 30 min. (b) For 13a → 34–36, 41: Fe, AcOH, EtOH, 80 °C, 2.5 h.

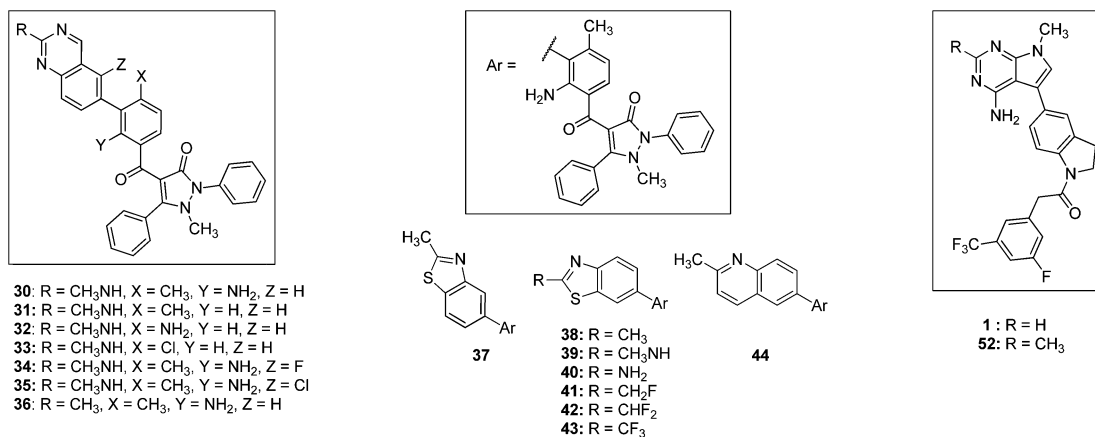
Scheme 7. Synthesis of PERK Inhibitor 52^a

^aReagents and conditions: (a) 45, CDI, THF, 60 °C, 2 h, then 46, rt, 20 h; (b) bis(pinacolato)diboron, Pd(dppf)₂Cl₂·CH₂Cl₂, KOAc, 1,4-dioxane, 90 °C, 16 h; (c) NaH, CH₃I, DMF, 0 °C → rt, 16 h; (d) NH₃, 1,4-dioxane, water, 135 °C (microwave), 2 h; (e) Pd(PPh₃)₄, K₃PO₄, toluene, MeOH, water, 110 °C (microwave), 20 min.

ELISA assay looking at cellular inhibition of PERK autophosphorylation (using a phospho-PERK T980 (pPERK) specific antibody in HT1080 cells stably transfected with doxycycline-inducible T-REx-PERK-FLAG)²¹ and a functional imaging assay looking at the rescue of bulk protein synthesis in stressed U2OS cells (incorporation of the methionine analog *L*-azidohomoalanine into protein in methionine-starved media with thapsigargin-induced ER stress; imaging via click chemistry²² with an AlexaFluor 488 alkyne dye). Hits were also counterscreened against the other known eIF2 α kinases (general control nonderepressible 2 (GCN2), protein kinase RNA-activated (PKR), and heme-regulated eIF2 α kinase (HRI)), and IRE-1 (the mediator of an alternative ER-stress pathway). Two series of compounds stood out from the screen, represented by compounds 7 (PERK IC₅₀ = 41 nM) and 10a/10b (PERK IC₅₀ = 4/42 nM). Both series demonstrated good cellular activity but had significant inhibitory activity against

GCN2 (Table 1). GCN2 shares close homology with PERK in the kinase domain, and since it mediates a different stress-response pathway in response to amino acid starvation or UV damage (also signaling through eIF2 α), the GCN2 activity posed a potential problem for evaluating on-target effects of PERK inhibition. Neither series inhibited IRE-1 (IC₅₀ > 50 μ M), and selectivity over PKR and HRI was not an issue (7: PKR IC₅₀ > 10 μ M; HRI IC₅₀ > 10 μ M. 10a: PKR IC₅₀ = 480 nM; HRI IC₅₀ > 10 μ M).

Compound 7 originated from a prior B-Raf inhibitor program and, as might be expected, had significant activity in B-Raf mediated assays¹⁴ (B-Raf IC₅₀ = 8 nM; A375 pPERK IC₅₀ = 11 nM). Apart from the B-Raf activity, 7 was moderately selective over other kinases in a kinase inhibition panel screen (Table 1). Given our prior experience with B-Raf inhibitors enhancing the proliferation of certain cell lines,²³ our primary objective with this series was to completely remove the B-Raf

Table 1. In Vitro Data for PERK Inhibitors 1, 7, 10a, 30–44, and 52^a

| compd | enzyme assay | | | cellular assay | | | | | kinase selectivity | |
|-------|-------------------------------|-------------------------------|--------------------------------|--------------------------------|--|---------------------------------------|--------------------------------|---------------------------------------|---------------------------------------|-----------------------------|
| | PERK IC ₅₀ (nM) | GCN2 IC ₅₀ (nM) | B-Raf IC ₅₀ (nM) | pPERK IC ₅₀ (nM) | protein synthesis rescue EC ₅₀ (nM) | PERK CHoP IC ₅₀ (nM) | pGCN2 IC ₅₀ (nM) | GCN2 CHoP IC ₅₀ (nM) | selectivity ratio ^b (%) | number of kinases tested |
| 1 | 1 | 3900 | >1000 | 6 | 13 | 20 | nd | >50000 | 6 | 387 |
| 7 | 41 | 420 | 8 | 65 | 310 | 1200 | nd | 640 | 27 | 100 |
| 10a | 4 | 290 | >1000 | nd | 520 | nd | nd | nd | nd | |
| 30 | 3 | 42 | 300 | 12 | 130 | 480 | 17 | 550 | 16 | 100 |
| 31 | 1 | 5 | 8 | 110 | 310 | 480 | nd | 140 | 24 | 100 |
| 32 | 3 | 12 | 66 | 45 | 640 | 320 | nd | 240 | 17 | 100 |
| 33 | 5 | 10 | 13 | 140 | 280 | 1000 | nd | 120 | 20 | 100 |
| 34 | 4 | 36 | >1000 | 30 | 130 | 400 | nd | 520 | 9 | 381 |
| 35 | 6 | 42 | >1000 | 59 | 200 | 650 | nd | 1100 | 5 | 100 |
| 36 | 5 | 240 | >1000 | 35 | 180 | 2300 | nd | 6000 | 4 | 100 |
| 37 | 240 | >10000 | >1000 | >10000 | 5600 | nd | nd | nd | nd | |
| 38 | 4 | 1400 | >1000 | 20 | 190 | 320 | 520 | >50000 | 2 | 100 |
| 39 | 9 | 97 | >1000 | 82 | 200 | 760 | 50 | 1300 | 2 | 387 |
| 40 | 11 | 100 | >1000 | 41 | 210 | 1100 | 44 | 1200 | 4 | 100 |
| 41 | 6 | 310 | >1000 | 65 | 170 | 2100 | 53 | 3700 | 0 | 100 |
| 42 | 11 | 610 | >1000 | 86 | 290 | 4800 | 79 | 1900 | 0.3 | 387 |
| 43 | 53 | >50 000 | >1000 | 88 | 1300 | 3000 | >50000 | >50000 | 1 | 100 |
| 44 | 6 | 7300 | >1000 | 84 | 400 | 770 | >50000 | >50000 | 0 | 387 |
| 52 | 2 | >50000 | >1000 | 12 | 52 | 89 | nd | >50000 | 0.5 | 387 |

^aData represent an average of at least two determinations. nd: not determined. ^bKINOMEScan: percentage of tested kinases with >65% inhibition at 1 μM test concentration.

inhibitory activity while maintaining or improving the activity against PERK. The inhibitors **10a,b** came from a prior c-MET inhibitor program¹⁶ (**10a/10b**: c-MET IC₅₀ = 6/1 nM). This series had moderate selectivity over other kinases (**10b**: >65% inhibition of 10 out of 47 kinases tested at 1 μM), and the main objective for optimization was to maintain the excellent activity against PERK while improving upon the kinase selectivity.

Among the optimization strategies available, combining structural features of **7** and **10a,b** into a hybrid molecule proved to be particularly successful (Figure 2). Cocrystal structures of **7** and **10b** were obtained with PERK, and the inhibitors were both observed to bind to the inactive DFG-out²⁴ conformation of the protein. Overlay of the cocrystal structures of **7** and **10b** with PERK indicated almost identical alignment of the amide carbonyls of the two inhibitors with PERK, and the hybrid structure **30** was therefore suggested from the 10-fold greater potency of **10a** compared with **10b** against PERK (4 nM vs 42 nM). Compound **30** maintained good activity against PERK (Table 1), and it had good overall kinase selectivity and microsomal stability (rat CL_{int} = 29 μL

min⁻¹ mg⁻¹). Compound **30** retained some residual B-Raf activity at a level that was found to be sufficient to still cause activation of MAPK signaling in sensitive cell lines (EC₅₀ = 190 nM in MIA PaCa-2 cells),²³ and activity against GCN2 was also substantially increased resulting in only a 12-fold selectivity window for PERK over GCN2 at the enzyme level.

The problematic inclusion of GCN2 inhibitory activity, with its attendant consequences for complicating interpretation of the functional activity of dual PERK/GCN2 inhibitors, led to the exploration of assays to give a cellular readout of the GCN2 inhibition being observed (Table 1). A MSD assay was developed for phospho-GCN2 (pGCN2) giving a direct mechanistic readout of endogenous GCN2 autophosphorylation in HT1080 cells stimulated by amino acid starvation. A CHoP bDNA assay (HT1080 cell line) was also developed for measuring the relative downstream pathway effects of PERK and GCN2 inhibition for dual PERK/GCN2 inhibitors such as **30**. The PERK pathway was activated with thapsigargin and the GCN2 pathway was separately activated by amino acid starvation, both resulting in CHoP mRNA expression by

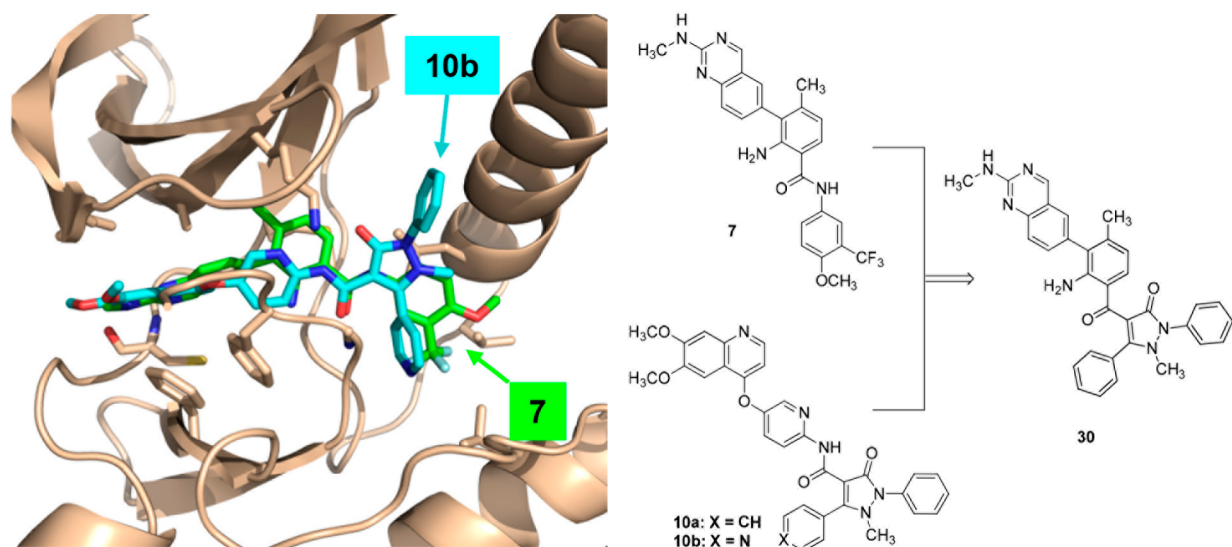


Figure 2. Design of a hybrid series of PERK inhibitors. Overlay of cocrystal structures of 7 and 10b with PERK suggested hybrid structure 30.

signaling through ATF4. The inhibitory effect of compounds on CHO_P mRNA expression resulting from either PERK inhibition or GCN2 inhibition could then be measured. As can be seen from Table 1, downstream signaling through ATF4 appears to be more sensitive to GCN2 inhibition than PERK inhibition (cf. PERK CHO_P vs GCN2 CHO_P). Thus, compound 30 is equipotent at inhibiting PERK and GCN2 autophosphorylation and is similarly equipotent at inhibiting CHO_P mRNA expression through the PERK and GCN2 pathways, despite having some selectivity at the PERK/GCN2 enzyme level.

A brief exploration of substituent SAR around the central benzoyl ring was performed first. Deletion of the amino group (31) had a modest effect on PERK activity but increased off-target GCN2 and B-Raf activity and led to poor microsomal stability (rat $CL_{int} = 497 \mu\text{L min}^{-1} \text{mg}^{-1}$). Swapping the methyl group for an amino group (32) or a chloro group (33) again had a minimal effect on PERK activity, but activity against GCN2 and B-Raf was substantial for both compounds and 33 again had relatively poor microsomal stability (rat $CL_{int} = 167 \mu\text{L min}^{-1} \text{mg}^{-1}$).

The upper aminoquinazoline fragment of 30 proved to be the most fruitful area for SAR exploration. The 5-fluoroquinazoline 34 and 5-chloroquinazoline 35 had substantially reduced activity against B-Raf while maintaining PERK activity. Compounds 34 and 35 also demonstrated improved selectivity against a broad panel of kinases (Table 1). A cocrystal structure of 34 with PERK (Figure 3) illustrates the binding mode of this series in the ATP binding site of the PERK kinase domain. The protein adopts a conformation in which the activation loop is folded out (DFG-out),²⁴ with the 5-phenyl substituent of the pyrazolone occupying the DFG-out pocket. The 2-phenyl substituent of the pyrazolone occupies a pocket adjacent to the α C-helix of the kinase. The pyrazolone carbonyl forms a hydrogen bond with the catalytic lysine (Lys622). The benzoyl carbonyl forms a hydrogen bond with the backbone N–H of the DFG Asp955, and the aminoquinazoline moiety forms hydrogen bonds to the kinase hinge region Cys891. The source of the improved PERK/B-Raf selectivity of 34 and 35 relative to 30 arises from the difference in the gatekeeper residue between the two kinases. PERK has a

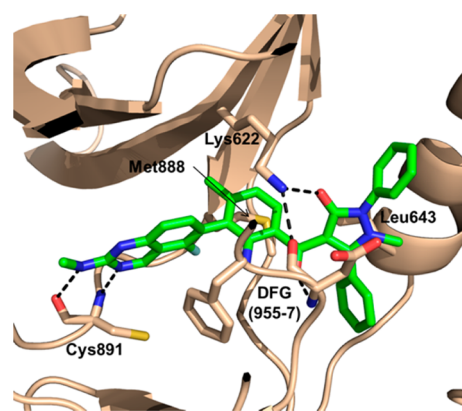


Figure 3. Cocrystal structure of 34 solved in complex with PERK at 1.8 Å resolution.

methionine gatekeeper residue (Met888) that accommodates small substituents from the quinazoline 5-position; the side chain of the corresponding threonine gatekeeper residue of B-Raf does not.

Compounds 36–39 represent a key progression in SAR around the quinazoline hinge-binder. First, replacing the 2-methylamino substituent of the quinazoline 30 with a 2-methyl substituent (36) retained PERK activity but was detrimental to GCN2 activity. Second, our cocrystal structural data suggested that the quinazoline moiety of compounds such as 34 had the potential to adopt two alternative binding modes with either quinazoline ring N atom capable of hydrogen-bonding to the Cys891 backbone N–H. This was explored by changing the hinge-binding heterocycle to the benzothiazole 37 (designed to place the benzothiazole N in proximity to the Cys891 N–H by analogy with 34, Figure 3). Compound 37 had poor PERK activity, but switching the point of attachment of the benzothiazole to the benzoyl core in order to give access to the alternative binding mode was well-accommodated by PERK. Thus, benzothiazole 38 maintained excellent activity against PERK and demonstrated good selectivity against GCN2, B-Raf, and a broad panel of other kinases. Reinstalling the 2-methylamino substituent on the benzothiazole (39) restored activity against GCN2 but retained excellent selectivity

against a broad panel of kinases. Compound **40** was identified as the primary circulating metabolite of **39** in rodent studies, and it had a very similar in vitro profile to **39**.

A cocrystal structure of **39** with PERK (Figure 4) revealed that while the general binding mode to PERK was similar to

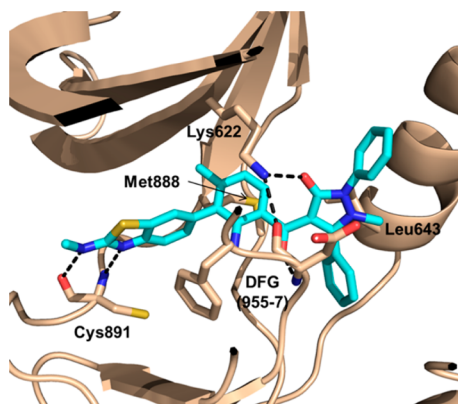


Figure 4. Cocrystal structure of **39** solved in complex with PERK at 1.9 Å resolution.

that of **34**, the benzo-fused ring of the benzothiazole moiety adopted the previously noted alternative binding mode and was pushed much further back toward the gatekeeper residue (Met888) compared with **34**, thus accounting for the very high selectivity of **39** over other kinases.

The fluorinated analogs **41–43** were prepared as part of the SAR exploration of **38**. Both the monofluoro- and difluoromethyl analogs **41** and **42** were found to be functionally balanced dual PERK/GCN2 inhibitors. The inhibitor **42** had superb selectivity over other kinases and excellent rat pharmacokinetic properties (Table 2). By contrast, the

Table 2. In Vivo Pharmacokinetic Properties of PERK Inhibitors^a

| compd | species | iv (1 mg/kg) ^b | | | po | |
|------------|---------|---------------------------|---------------|------------------------|-------------------|-----------------|
| | | MRT (h) | CL (L/(h·kg)) | V _{ss} (L/kg) | AUC (μM·h) | F (%) |
| 1 | rat | 3.7 | 0.29 | 1.0 | 8.2 ^c | 44 ^c |
| 10a | rat | 10.4 | 0.07 | 0.73 | 20.2 ^d | 50 ^d |
| 32 | rat | 0.5 | 1.0 | 0.56 | 0.8 ^e | 18 ^e |
| 34 | rat | 3.9 | 0.57 | 2.2 | 3.8 ^c | 48 ^c |
| 35 | rat | 5.5 | 0.50 | 2.7 | 3.7 ^c | 49 ^c |
| 36 | rat | 1.4 | 2.2 | 2.6 | 1.2 ^c | 69 ^c |
| 38 | rat | 2.2 | 1.4 | 3.1 | 0.1 ^c | 3 ^c |
| 39 | rat | 3.1 | 0.64 | 2.0 | 2.5 ^c | 35 ^c |
| 40 | rat | 2.2 | 3.0 | 6.5 | 1.0 ^c | 67 ^c |
| 42 | rat | 5.3 | 0.94 | 5.0 | 3.4 ^c | 76 ^c |
| 43 | rat | 10.8 | 0.75 | 8.1 | 3.2 ^c | 83 ^c |
| 44 | rat | 2.3 | 1.6 | 3.6 | 1.4 ^c | 55 ^c |
| 44 | mouse | 5.0 | 0.25 | 1.2 | 8.8 ^c | 46 ^c |
| 52 | rat | 11.9 | 0.10 | 1.2 | 23.6 ^c | 98 ^c |

^aCompounds dosed in male Sprague–Dawley rats and male CD-1 mice. ^bCompound dosed iv as a DMSO solution. ^cCompound dosed as a solution at 2.5 mg/kg po in 1% Pluronic F68/1% HPMC/15% Captisol/83% H₂O, pH 2.0, with MsOH. ^dCompound dosed as a solution at 2.0 mg/kg po in 1% Tween 80/99% OraPlus. ^eCompound dosed as a solution at 2.5 mg/kg po in 1% Tween 80/2% HPMC/97% H₂O, pH 2.0, with MsOH.

trifluoromethyl analog **43** was identified as a selective PERK inhibitor devoid of measurable GCN2 activity. Selectivity over other kinases and rat pharmacokinetic properties were both excellent for **43**.

The final piece of SAR around the kinase hinge-binding moiety involved changing the 2-methylbenzothiazole of **38** for the analogous 2-methylquinoline of **44**. Compound **44** was an equally potent PERK inhibitor in vitro, with 1000-fold selectivity over GCN2 and with no measurable effects due to GCN2 inhibition in the cellular assays. It had exquisite selectivity over a large panel of kinases, and while the rat pharmacokinetic properties were only moderate, the mouse pharmacokinetic properties were significantly better (Table 2). Oral bioavailability of **44** in rat (and mouse) was significantly improved compared with that of **38**, making it a superior in vivo tool compound. A cocrystal structure of **44** with PERK (Figure 5a) revealed that the quinoline methyl group projects toward the hinge Cys891 carbonyl and the distance (3.4 Å) is suggestive of a hydrogen bond between a methyl C–H and the carbonyl oxygen.²⁵ The source of the selectivity imparted by the quinoline methyl group of **44** over GCN2 is suggested by comparing the apo structures²⁶ of mouse PERK²⁷ and yeast GCN2²⁸ (Figure 5b), where it is evident that the hinge Cys residues of the two proteins adopt different conformations in the apo state. If this difference translates to the protein structure with inhibitor bound, it would place the hinge Cys carbonyl of GCN2 closer to the quinoline methyl group of **44**, leading to an unfavorable interaction.

Disclosure of the first potent, selective PERK inhibitors by Axten^{12,13} (Figure 1) was contemporaneous with our identification of **44** as a potent, selective PERK inhibitor. We prepared the analog **1** as a benchmark and confirmed its activity (Table 1). The cocrystal structures of this series^{12,13} with PERK indicated a conformation of the kinase region different from that observed with our inhibitors, with the activation loop folded in (DFG-in). However, these structures clearly indicated that the addition of a methyl group to the 2-position of the 7H-pyrrolo[2,3-d]pyrimidine would be accommodated by the protein in a manner similar to the 2-methylquinoline substituent of **44**. We wondered if this substitution would further improve upon the already good kinase selectivity of **1** (Table 1) in an analogous manner to the improvement observed with **30** → **36**. Compound **52** was therefore prepared and profiled. While compound **52** was marginally less potent in vitro when compared with **1**, the kinase selectivity profile was significantly improved and it had an outstanding rat pharmacokinetic profile (Table 2). The cocrystal structure of **52** with PERK (Figure 6) confirmed the proposed role of the additional methyl group, with a distance of 3.2 Å between the methyl group and Cys891 strongly suggestive of a hydrogen bond similar to the observation with **44**. It should be noted that both **1** and **52** are significantly more potent in the PERK cellular assays compared with the compounds described in the pyrazolone series, despite having apparently similar PERK enzyme inhibitory activities. This may be a reflection of these compounds reaching the lower readout limit in the PERK enzyme assay due to the 1 nM concentration of PERK protein used in the enzyme assay.

Pharmacology. The pharmacokinetic data presented in Table 2 for key compounds demonstrate that the PERK inhibitors were generally well behaved in vivo with good bioavailability, duration, and exposure. The good pharmacokinetic properties of the molecules facilitated in vivo pharmaco-

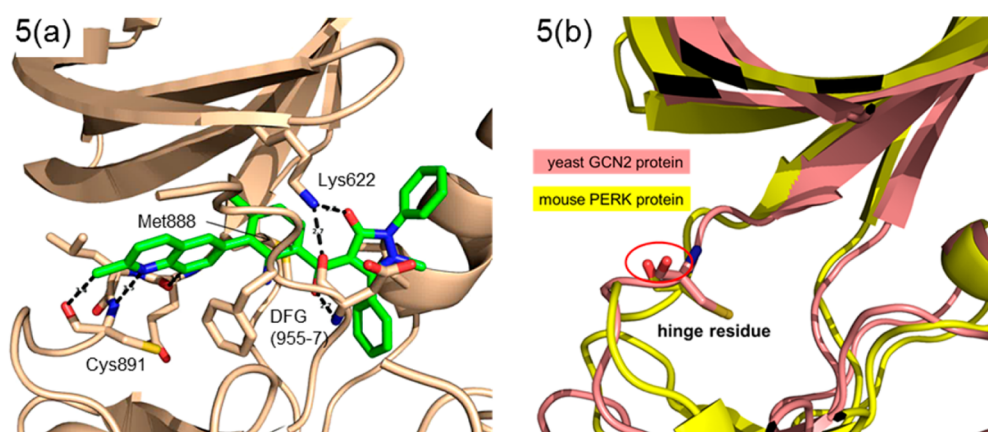


Figure 5. (a) Cocystal structure of **44** solved in complex with PERK at 2.4 Å resolution. (b) Overlay of apo mouse PERK and apo yeast GCN2 crystal structures demonstrating different conformations of the hinge Cys residue of the two proteins in the apo state (circled in red).

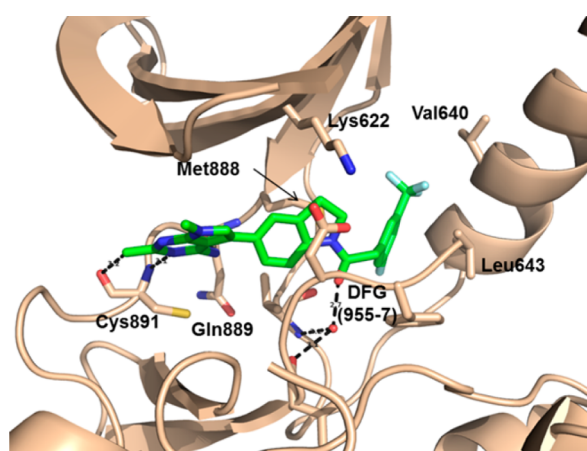


Figure 6. Cocystal structure of **52** solved in complex with PERK at 2.7 Å resolution.

logical evaluation of the compounds. Compounds were generally well tolerated upon repeat dosing.

A pharmacodynamic (PD) model for measuring in vivo PERK inhibition was established in athymic nude mice implanted with a doxycycline-inducible HT1080–T-REx–PERK–FLAG Matrigel plug. The mice were dosed with doxycycline in their drinking water overnight prior to implantation, causing overexpression of PERK in the HT1080 plug. The mice were dosed orally with inhibitors, and the tumor plug was removed at predetermined time points postdose, and the inhibition of PERK autophosphorylation was measured (comparing pPERK/total PERK ratios). Dose–response PD data at the 4 h time point are shown in Figure 7 for the selective PERK inhibitors **44** and **52**. Compound **44** robustly inhibited PERK autophosphorylation in this assay ($ED_{50} \approx 3$ mg/kg; $ED_{90} \approx 60$ mg/kg at the 4 h time point), and >50% target coverage was maintained for 24 h in a time course PD assay when dosed at 100 mg/kg po. Compound **52** was more potent than **44** in the PD assay ($ED_{50} \approx 2$ mg/kg; $ED_{90} \approx 30$ mg/kg at the 4 h time point), with >50% target coverage being maintained for 24 h in the time course PD assay when dosed at 3 mg/kg po (reflecting the low clearance of **52**).

CONCLUSION

In summary, we have described the design, synthesis, biochemical, and pharmacological properties of a series of

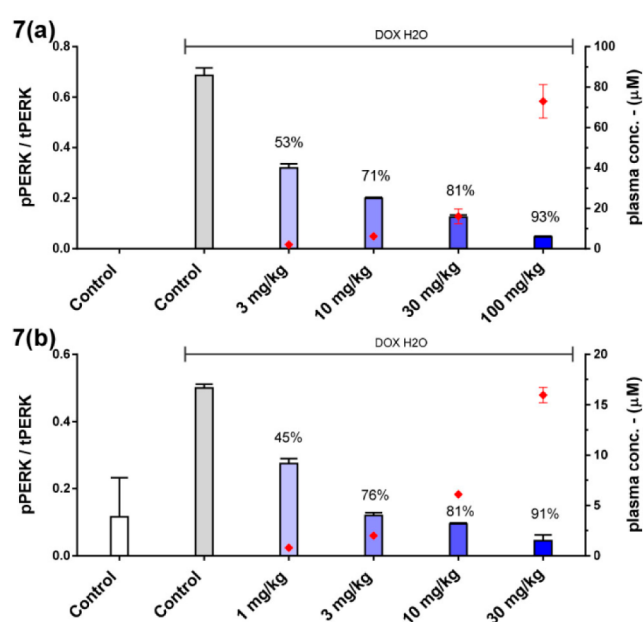


Figure 7. Inhibition of PERK autophosphorylation 4 h postdose in doxycycline-inducible PERK HT1080 PD assay with inhibitors dosed orally: (a) **44** at 3, 10, 30, 100 mg/kg; (b) **52** at 1, 3, 10, 30 mg/kg. $n = 3$ mice per group. Controls are Matrigel plugs (vehicle dosing) in the absence and presence of doxycycline.

1*H*-pyrazol-3(2*H*)-one PERK inhibitors. Structural information was used to optimize potency and selectivity resulting in the identification of **44** as a potent, exquisitely selective PERK inhibitor. Following from the information learned in deriving **44**, the PERK inhibitor **52** was designed to improve upon the selectivity of the recently disclosed PERK inhibitor **1**. Compounds **44** and **52** are structurally dissimilar selective PERK inhibitors, binding to different conformations of the PERK kinase domain. Both compounds demonstrated excellent pharmacokinetic properties and were able to give good PERK target coverage in mouse PD studies. The use of these compounds for exploration of PERK pathway biology and PERK target validation, both in vitro and in vivo, will be described elsewhere.

EXPERIMENTAL SECTION

Chemistry. Reactions were run under inert atmosphere (nitrogen or argon) and were stirred using a PTFE-coated magnetic stir bar

unless noted otherwise. Reactions run at elevated temperature were performed using a magnetic hot plate stirrer at the temperature indicated utilizing an oil bath, aluminum heating block, or aluminum beads for heat transfer. Microwave reactions were run either in a Biotage microwave reactor set to normal power at the indicated temperature or in a CEM Discover microwave reactor equipped with the PowerMAX feature and were performed in sealed microwave reaction vessels. Solvents and reagents obtained from commercial sources were used without further purification. Solutions were concentrated using a rotary evaporator, and solids were collected by filtration using either a Büchner funnel or sintered funnel. Residual solvent was removed from products using a vacuum manifold maintained at approximately 1 Torr. All yields reported are isolated yields after removal of residual solvents.

Silica gel chromatography refers either to column chromatography as described by Still²⁹ using EMD silica gel 60 (230–400 mesh) as the stationary phase or to the use of an automated medium pressure liquid chromatography system (Teledyne ISCO or Shoko Scientific Purif-Espoir2) using prepacked silica gel cartridges (RediSep, Interchim PuriFlash, or SiliCycle). The eluent solvent systems and gradients are as noted.

¹H, ¹⁹F, and ¹³C NMR spectra were obtained on a Bruker BioSpin GmbH magnetic resonance spectrometer. NMR spectra are reported as chemical shifts in parts per million (ppm) relative to an internal solvent reference. High resolution mass spectra were acquired on a Synapt G2 HDMS instrument (Waters Corporation, Manchester, U.K.) operated in positive electrospray ionization mode.

Analytical HPLC–MS was conducted using an Agilent 1100 series HPLC–mass spectrometry instrument and a Zorbax SB-C18 column (50 mm × 3.0 mm, 3.5 μm) at 40 °C with a gradient of 5–95% MeCN/water (modified with 0.1% TFA) over 3 min and a 1.5 mL/min flow rate. Flow from the UV detector was split (50:50) to the MS detector, which was configured with an API-ES source. Purities for final compounds were measured using UV detection at 254 and 215 nm and were ≥95%.

All synthetic starting materials and reagents either were from commercial sources or were synthesized according to the referenced literature procedures.

1-(5-(4-Amino-7-methyl-7H-pyrrolo[2,3-d]pyrimidin-5-yl)-indolin-1-yl)-2-(3-fluoro-5-(trifluoromethyl)phenyl)ethanone (1). The title compound was prepared as described by Axten.¹² ¹H NMR (400 MHz, DMSO-*d*₆): δ 8.16 (s, 1H), 8.12 (d, *J* = 8.2 Hz, 1H), 7.56–7.62 (m, 2H), 7.52 (d, *J* = 9.8 Hz, 1H), 7.34 (s, 1H), 7.21–7.29 (m, 2H), 6.07 (br s, 2H), 4.27 (t, *J* = 8.4 Hz, 2H), 4.07 (s, 2H), 3.74 (s, 3H), 3.27 (t, *J* = 8.3 Hz, 2H). ¹⁹F NMR (377 MHz, DMSO-*d*₆): δ –61.09 (s, 3F), –111.75 (s, 1F). ¹³C NMR (100 MHz, DMSO-*d*₆): δ 168.0, 162.9, 160.5, 157.1, 151.6, 150.4, 141.7, 140.1, 132.8, 129.9, 127.1, 124.9, 124.0, 123.0, 121.4, 121.1, 116.2, 114.9, 110.9, 99.9, 47.8, 40.8, 30.7, 27.5. HRMS (ESI) *m/z* calculated for C₂₄H₁₉F₄N₅O + H⁺ [*M* + H⁺]: 470.1604. Found: 470.1601.

2-Amino-3-iodo-*N*-(4-methoxy-3-(trifluoromethyl)phenyl)-4-methylbenzamide (5). A solution of 3-iodo-4-methyl-2-nitrobenzoic acid (**2**) (1.052 g, 3.43 mmol) and 4-methoxy-3-(trifluoromethyl)aniline (**3**) (0.720 g, 3.77 mmol) in DMF (20 mL) was treated with *i*-Pr₂NEt (0.72 mL, 4.11 mmol) followed by TBTU (1.32 g, 4.11 mmol), and the mixture was stirred at rt for 2 h. The reaction mixture was added dropwise to stirred saturated aqueous NaHCO₃ (100 mL). A tan precipitate formed. The mixture was stirred for 30 min, and the solid was collected by filtration, washing with water. The solid was suspended in DMF (40 mL), heated to dissolve, and added dropwise to stirred 0.5 M aqueous HCl (250 mL). The resulting precipitate was collected by filtration, washed with water, and dried to give 3-iodo-*N*-(4-methoxy-3-(trifluoromethyl)phenyl)-4-methyl-2-nitrobenzamide (**4**) as a pale pink solid. HPLC–MS (ESI) *m/z* calculated for C₁₆H₁₂F₃IN₂O₄ + H⁺ [*M* + H⁺]: 481.0. Found: 480.8.

The crude **4** (1.65 g, 3.43 mmol) was suspended in EtOH (25 mL) and AcOH (2.0 mL, 34 mmol). The mixture was heated at gentle reflux until dissolved and then treated with iron powder (0.765 g, 13.7 mmol). The resulting mixture was heated at gentle reflux for 3 h. The

reaction mixture was allowed to cool to rt and was then diluted with 2 N aqueous HCl (50 mL) and stirred for 30 min. The mixture was diluted with water (100 mL) and extracted with EtOAc (3 × 100 mL). The combined EtOAc extracts were washed with saturated aqueous NaHCO₃ (200 mL), re-extracting the aqueous layer with EtOAc (100 mL). The combined EtOAc extracts were concentrated, and the resulting solid was suspended in DCM (5 mL) and sonicated. The solid was collected by filtration, washing with DCM (1 mL), to give **5** (1.20 g, 78% yield) as a pale-pink solid. ¹H NMR (400 MHz, DMSO-*d*₆): δ 10.22 (s, 1H), 8.04 (d, *J* = 2.5 Hz, 1H), 7.93 (dd, *J* = 2.5, 9.1 Hz, 1H), 7.62 (d, *J* = 7.8 Hz, 1H), 7.27 (d, *J* = 9.0 Hz, 1H), 6.70 (d, *J* = 8.2 Hz, 1H), 6.46 (s, 2H), 3.88 (s, 3H), 2.40 (s, 3H). HPLC–MS (ESI) *m/z* calculated for C₁₆H₁₄F₃IN₂O₂ + H⁺ [*M* + H⁺]: 451.0. Found: 450.8.

2-Amino-*N*-(4-methoxy-3-(trifluoromethyl)phenyl)-4-methyl-3-(2-(methylamino)quinazolin-6-yl)benzamide (7). A microwave reactor vessel was charged with **5** (0.196 g, 0.435 mmol), *N*-methyl-6-(4,4,5,5-tetramethyl-1,3,2-dioxaborolan-2-yl)quinazolin-2-amine (**6**)¹⁴ (0.161 g, 0.566 mmol), Na₂CO₃·H₂O (0.162 g, 1.31 mmol), PdCl₂(PPh₃)₂ (0.0153 g, 0.0218 mmol), and 10:1 DMF/H₂O (1.8 mL). The vessel was sealed and heated at 150 °C for 15 min in a microwave reactor. The reaction mixture was diluted with water, neutralized with TFA, and extracted with EtOAc. The organic extracts were washed with water and brine and then dried over Na₂SO₄. The solution was concentrated in vacuo, and the resulting residue was purified by silica gel chromatography, eluting with a gradient of 20–80% EtOAc/hexanes. The product fractions were combined, concentrated, and slurried in 10:1 Et₂O/hexanes. The solid was collected by filtration to give **7** (0.142 g, 68% yield) as an off-white solid. ¹H NMR (400 MHz, DMSO-*d*₆): δ 10.15 (s, 1H), 9.13 (s, 1H), 8.08 (d, *J* = 2.5 Hz, 1H), 7.96 (dd, *J* = 2.5, 9.0 Hz, 1H), 7.58–7.71 (m, 3H), 7.48 (dd, *J* = 1.9, 8.5 Hz, 1H), 7.37 (d, *J* = 4.5 Hz, 1H), 7.28 (d, *J* = 9.0 Hz, 1H), 6.67 (d, *J* = 8.2 Hz, 1H), 5.77 (s, 2H), 3.89 (s, 3H), 2.94 (d, *J* = 4.9 Hz, 3H), 1.98 (s, 3H). ¹⁹F NMR (377 MHz, DMSO-*d*₆): δ –60.80 (s, 3F). ¹³C NMR (100 MHz, DMSO-*d*₆): δ 167.9, 161.9, 160.3, 152.9, 147.2, 140.3, 136.67 (q, *J* = 288 Hz), 136.2, 132.1, 130.3, 129.0, 127.8, 127.0, 126.0, 125.0, 120.1, 119.0 (q, *J* = 6 Hz), 116.9, 116.47 (q, *J* = 30 Hz), 113.2, 113.1, 56.3, 40.2, 28.1, 20.7. HRMS (ESI) *m/z* calculated for C₂₅H₂₂F₃N₅O₂ + H⁺ [*M* + H⁺]: 482.1804. Found: 482.1800.

***N*-(5-(6,7-Dimethoxyquinolin-4-yl)oxy)pyridin-2-yl)-1-methyl-3-oxo-2,5-diphenyl-2,3-dihydro-1*H*-pyrazole-4-carboxamide (10a).** A mixture of 5-(6,7-dimethoxyquinolin-4-yl)oxy)pyridin-2-amine (**8**)¹⁶ (0.175 g, 0.589 mmol) and 1-methyl-3-oxo-2,5-diphenyl-2,3-dihydro-1*H*-pyrazole-4-carboxylic acid (**9a**)¹⁷ (0.208 g, 0.706 mmol) in DMF (5 mL) was treated with triethylamine (0.21 mL, 1.47 mmol) followed by HATU (0.336 g, 0.883 mmol). The mixture was stirred at 90 °C for 16 h. The mixture was allowed to cool to rt and was then diluted with water (60 mL) and stirred for 10 min. The precipitate was collected by filtration. The crude material was purified by silica gel chromatography, eluting with a gradient of 0–10% MeOH/DCM to give **10a** (0.105 g, 31% yield) as a tan solid. ¹H NMR (400 MHz, DMSO-*d*₆): δ 11.41 (s, 1H), 8.50 (d, *J* = 5.1 Hz, 1H), 8.34 (d, *J* = 2.7 Hz, 1H), 8.24 (d, *J* = 9.0 Hz, 1H), 7.53–7.75 (m, 12H), 7.42 (s, 1H), 6.53 (d, *J* = 5.3 Hz, 1H), 3.96 (s, 3H), 3.95 (s, 3H), 3.18 (s, 3H). ¹³C NMR (100 MHz, DMSO-*d*₆): δ 162.4, 159.7, 159.7, 155.0, 152.6, 149.4, 149.2, 148.8, 146.5, 146.4, 141.2, 132.8, 131.1, 130.4, 130.2, 129.5, 129.0, 128.2, 127.6, 127.1, 115.0, 114.3, 107.9, 103.1, 99.1, 97.9, 55.7, 55.7, 35.6. HRMS (ESI) *m/z* calculated for C₃₃H₂₇N₅O₅ + H⁺ [*M* + H⁺]: 574.2090. Found: 574.2087.

***N*-(5-(6,7-Dimethoxyquinolin-4-yl)oxy)pyridin-2-yl)-1-methyl-3-oxo-2-phenyl-5-(pyridin-4-yl)-2,3-dihydro-1*H*-pyrazole-4-carboxamide (10b).** **10b** was prepared as a yellow solid (165 mg, 16% yield) in an analogous manner to **10a** from **8** and 1-methyl-3-oxo-2-phenyl-5-(pyridin-4-yl)-2,3-dihydro-1*H*-pyrazole-4-carboxylic acid (**9b**).¹⁶ ¹H NMR (400 MHz, DMSO-*d*₆): δ 11.31 (s, 1H), 8.78–8.88 (m, 2H), 8.50 (d, *J* = 5.3 Hz, 1H), 8.34 (t, *J* = 8.3 Hz, 1H), 8.25 (s, 1H), 8.22–8.23 (m, 1H), 7.48–7.76 (m, 8H), 7.38–7.47 (m, 1H), 6.54 (t, *J* = 5.6 Hz, 1H), 3.96 (s, 3H), 3.95 (s, 3H), 3.21 (s, 3H). ¹³C NMR (100 MHz, DMSO-*d*₆): δ 161.9, 159.8, 159.5, 152.7, 151.5,

149.6, 149.6, 149.5, 149.1, 149.0, 148.7, 146.5, 146.2, 141.2, 135.7, 132.4, 131.2, 129.6, 129.4, 127.5, 127.5, 124.6, 124.5, 115.0, 114.4, 107.6, 103.1, 99.1, 98.3, 55.7, 55.7, 35.3. HPLC–MS (ESI) m/z calculated for $C_{32}H_{26}N_6O_3 + H^+$ [M + H⁺]: 575.2. Found: 575.2.

General Procedure for the Synthesis of Intermediates 13a–d. A suspension of 2,5-diphenyl-1H-pyrazol-3(2H)-one (**12**)¹⁸ (3.00 g, 12.7 mmol) and calcium hydroxide (2.20 equiv, 2.07 g, 27.9 mmol) in 1,4-dioxane (50 mL) was heated at 50 °C for 20 min. Acid chloride selected from **11a–d** (1.20 equiv, 15.2 mmol) was added portionwise over 5 min, and the mixture was then heated at 90 °C for 16 h. The mixture was allowed to cool to rt and was then extracted into EtOAc (3 × 100 mL) from saturated aqueous NaHCO₃ (100 mL). The combined organic extracts were dried over Na₂SO₄, filtered, and concentrated in vacuo. The resulting solid was dried under vacuum overnight and used without further purification.

The solid was mixed with methyl *p*-toluenesulfonate (20 equiv, 38.4 mL, 254 mmol) and heated at 170 °C for 3 h. The mixture was allowed to cool to rt, diluted with 1 N aqueous NaOH (250 mL), and extracted into EtOAc (3 × 150 mL). The combined organic extracts were dried over Na₂SO₄, filtered, and concentrated in vacuo. The crude material was purified by silica gel chromatography eluting with a gradient of 0–12% MeOH/DCM to give **13a–d**.

4-(3-Iodo-4-methyl-2-nitrobenzoyl)-1-methyl-2,5-diphenyl-1H-pyrazol-3(2H)-one (13a). Tan solid; yield 47% (3.24 g, 6.01 mmol). ¹H NMR (400 MHz, CDCl₃): δ 7.46–7.72 (m, 7H), 7.41 (s, 3H), 7.33–7.40 (m, 2H), 3.23 (s, 3H), 2.52 (s, 3H). HPLC–MS (ESI) m/z calculated for $C_{24}H_{18}IN_3O_4 + H^+$ [M + H⁺]: 540.0. Found: 539.7.

4-(3-Bromo-4-methylbenzoyl)-1-methyl-2,5-diphenyl-1H-pyrazol-3(2H)-one (13b). Tan solid; yield 70% (0.80 g, 1.79 mmol). ¹H NMR (400 MHz, CDCl₃): δ 7.97–8.06 (m, 1H), 7.78–7.83 (m, 1H), 7.30–7.59 (m, 9H), 7.01–7.30 (m, 2H), 3.19 (s, 3H), 2.39 (s, 3H). HPLC–MS (ESI) m/z calculated for $C_{24}H_{19}BrN_2O_2 + H^+$ [M + H⁺]: 447.1/449.1. Found: 446.7/448.7.

4-(3-Bromo-4-nitrobenzoyl)-1-methyl-2,5-diphenyl-1H-pyrazol-3(2H)-one (13c). Off-white solid; yield 89% (12.38 g, 25.9 mmol). ¹H NMR (400 MHz, CDCl₃): δ 8.16 (s, 3H), 7.97 (d, *J* = 8.2 Hz, 1H), 7.81 (d, *J* = 8.4 Hz, 1H), 7.60–7.41 (m, 10H), 3.28 (s, 3H). HPLC–MS (ESI) m/z calculated for $C_{23}H_{16}BrN_3O_4 + H^+$ [M + H⁺]: 478.0/480.0. Found: 477.9/479.9.

4-(3-Bromo-4-chlorobenzoyl)-1-methyl-2,5-diphenyl-1H-pyrazol-3(2H)-one (13d). Tan solid; yield 74% (0.52 g, 1.11 mmol). ¹H NMR (400 MHz, CDCl₃): δ 8.08–8.13 (m, 1H), 7.79–7.85 (m, 1H), 7.31–7.56 (m, 11H), 3.21 (s, 3H). HPLC–MS (ESI) m/z calculated for $C_{23}H_{16}BrClN_2O_2 + H^+$ [M + H⁺]: 467.0/469.0. Found: 467.1/469.1.

General Procedure for the Synthesis of Intermediates 14a and 14c. A solution of **13a** or **13c** (7.42 mmol) in AcOH (8.5 mL, 148 mmol) and EtOH (64 mL) was treated with iron powder (9.8 equiv, 4.06 g, 72.8 mmol) and heated at 80 °C for 1.5 h. The mixture was allowed to cool to rt and concentrated in vacuo. The residue was diluted with DCM (40 mL) and 2 M NH₃/MeOH (40 mL) and then filtered through diatomaceous earth washing with 1:1 DCM and 2 M NH₃/MeOH. The filtrate was concentrated in vacuo and purified by silica gel chromatography, eluting with a gradient of 0–6% (2 M NH₃/MeOH)/DCM to give **14a,c**.

4-(2-Amino-3-iodo-4-methylbenzoyl)-1-methyl-2,5-diphenyl-1H-pyrazol-3(2H)-one (14a). Tan solid; yield 76% (2.88 g, 5.65 mmol). ¹H NMR (300 MHz, CDCl₃): δ 7.77 (d, *J* = 8.2 Hz, 1H), 7.41–7.54 (m, 9H), 6.97 (s, 1H), 6.55–6.60 (m, 1H), 3.13 (s, 3H), 2.43 (s, 3H). HPLC–MS (ESI) m/z calculated for $C_{24}H_{20}IN_3O_2 + H^+$ [M + H⁺]: 510.1. Found: 510.0.

4-(4-Amino-3-bromobenzoyl)-1-methyl-2,5-diphenyl-1H-pyrazol-3(2H)-one (14c). Brown solid; yield 90% (10.42 g, 23.2 mmol). ¹H NMR (400 MHz, DMSO-*d*₆): δ 7.86 (d, *J* = 1.6 Hz, 1H), 7.61–7.54 (m, 5H), 7.52–7.46 (m, 5H), 7.41 (dt, *J* = 5.7, 3.0 Hz, 1H), 6.72 (d, *J* = 8.6 Hz, 1H), 6.23 (s, 2H), 3.10 (s, 3H). HPLC–MS (ESI) m/z calculated for $C_{23}H_{18}BrN_3O_2 + H^+$ [M + H⁺]: 448.1/450.1. Found: 448.0/449.9.

6-Bromo-5-chloroquinazolin-2-amine (16). A suspension of 3-bromo-2-chloro-6-fluorobenzaldehyde (**15**) (12.88 g, 54.2 mmol) and guanidine carbonate (12.16 g, 67.5 mmol) in NMP (200 mL) and *i*-Pr₂NEt (23.5 mL, 135 mmol) was heated at 140 °C for 2 h. The reaction mixture was allowed to cool to rt, poured into water (1 L), and treated with brine (100 mL). The precipitate was collected by filtration and washed with water to give **16** (13.32 g, 95% yield) as a tan solid. ¹H NMR (400 MHz, DMSO-*d*₆): δ 9.30 (s, 1H), 7.93 (d, *J* = 9.0 Hz, 1H), 7.34 (d, *J* = 9.0 Hz, 1H), 7.26 (s, 2H). HPLC–MS (ESI) m/z calculated for $C_8H_5BrClN_3 + H^+$ [M + H⁺]: 257.9/259.9. Found: 258.0/260.0.

6-Bromo-2,5-dichloroquinazoline (17b). A suspension of **16** (14.45 g, 55.9 mmol) in DCM (350 mL) and DMF (20 mL) was treated successively with *n*-Bu₄NCl (18.94 g, 68.1 mmol), (CH₃)₃SiCl (28.0 mL, 221 mmol), and *t*-BuON=O (20.0 mL, 168 mmol) (added dropwise over 25 min). The reaction mixture was stirred at room temperature for an additional 15 min and then heated at 50 °C for 1 h. The mixture was allowed to cool to rt and extracted into DCM (3 × 100 mL) from saturated aqueous NaHCO₃ (125 mL). The combined organic extracts were dried (Na₂SO₄) and concentrated to give **17b** (15.54 g, 100%) as a tan solid. ¹H NMR (400 MHz, CDCl₃): δ 9.68 (s, 1H), 8.13 (d, *J* = 9.2 Hz, 1H), 7.81 (d, *J* = 9.0 Hz, 1H). HPLC–MS (ESI) m/z calculated for $C_8H_3BrCl_2N_2 + H^+$ [M + H⁺]: 276.9/278.9. Found: 276.7/278.7.

General Procedure for the Synthesis of Intermediates 18a,b. A suspension of **17a** (Aurum PharmaTech) or **17b** (56 mmol) in EtOH (125 mL) and methylamine (33% solution in EtOH, 37.5 mL, 300 mmol) was heated at 80 °C for 1 h in a sealed tube. The mixture was allowed to cool to rt and diluted with water (300 mL). The solid was collected by filtration and purified by silica gel chromatography, eluting with a gradient of 0–2.5% MeOH/DCM to give **18a,b**.

6-Bromo-5-fluoro-N-methylquinazolin-2-amine (18a). White solid; yield 100% (2.06 g, 8.04 mmol). ¹H NMR (400 MHz, CDCl₃): δ 9.22 (br s, 1H), 7.73 (dd, *J* = 9.0, 7.6 Hz, 1H), 7.32 (d, *J* = 9.2 Hz, 1H), 5.47 (br s, 1H), 3.14 (s, 3H). HPLC–MS (ESI) m/z calculated for $C_9H_7BrFN_3 + H^+$ [M + H⁺]: 256.0/258.0. Found: 255.9/257.9.

6-Bromo-5-chloro-N-methylquinazolin-2-amine (18b). Off-white solid; yield 57% (8.74 g, 32.1 mmol). ¹H NMR (400 MHz, CDCl₃): δ 9.34 (s, 1H), 7.80 (d, *J* = 9.0 Hz, 1H), 7.41 (d, *J* = 8.8 Hz, 1H), 5.42 (br s, 1H), 3.13 (d, *J* = 5.1 Hz, 3H). HPLC–MS (ESI) m/z calculated for $C_9H_7BrClN_3 + H^+$ [M + H⁺]: 272.0/274.0. Found: 271.9/274.0.

6-Bromo-2-methylquinazoline (18c). **18c** was acquired from commercial sources (Akos Building Blocks).

General Procedure for the Synthesis of Intermediates 19a–c. A suspension of an aryl bromide selected from **18a–c** (8.04 mmol), bis(pinacolato)diboron (1.13 equiv, 2.31 g, 9.11 mmol), Pd(dppf)₂Cl₂·CH₂Cl₂ (0.10 equiv, 646 mg, 0.79 mmol), and KOAc (3.9 equiv, 3.10 g, 31.6 mmol) in 1,4-dioxane (80 mL) was heated at 110 °C for 2.5 h and then allowed to cool to rt. The reaction mixture was filtered through a pad of diatomaceous earth, washing with DCM and MeOH. The filtrate was concentrated and purified by silica gel chromatography, eluting with a gradient of 20–100% EtOAc/hexanes to give **19a–c**.

5-Fluoro-N-methyl-6-(4,4,5,5-tetramethyl-1,3,2-dioxaborolan-2-yl)quinazolin-2-amine (19a). Off-white solid; yield 99% (2.41 g, 7.95 mmol). ¹H NMR (400 MHz, CDCl₃): δ 9.25 (br s, 1H), 7.94 (t, *J* = 7.5 Hz, 1H), 7.36 (d, *J* = 8.2 Hz, 1H), 5.47 (br s, 1H), 3.14 (d, *J* = 5.1 Hz, 3H) 1.39 (s, 12H). HPLC–MS (ESI) m/z calculated for $C_{15}H_{19}BFN_3O_2 + H^+$ [M + H⁺]: 304.2. Found: 222.1 (consistent with hydrolysis of boronate ester).

5-Chloro-N-methyl-6-(4,4,5,5-tetramethyl-1,3,2-dioxaborolan-2-yl)quinazolin-2-amine (19b). Yellow solid; yield 77% (1.33 g, 4.16 mmol). ¹H NMR (400 MHz, CDCl₃): δ 9.44 (br s, 1H), 7.93 (d, *J* = 8.6 Hz, 1H), 7.48 (d, *J* = 8.6 Hz, 1H), 5.45 (br s, 1H), 3.15 (d, *J* = 5.1 Hz, 3H), 1.40 (s, 12H). HPLC–MS (ESI) m/z calculated for $C_{15}H_{19}BClN_3O_2 + H^+$ [M + H⁺]: 320.1. Found: 320.2.

2-Methyl-6-(4,4,5,5-tetramethyl-1,3,2-dioxaborolan-2-yl)quinazoline (19c). Off-white solid; yield 100% (461 mg, 1.71 mmol). ¹H NMR (400 MHz, CDCl₃): δ 9.35 (s, 1H), 8.41 (s, 1H), 8.25 (d, *J* =

8.6 Hz, 1H), 7.93 (d, $J = 8.6$ Hz, 1H), 2.92 (s, 3H), 1.40 (s, 12H). HPLC–MS (ESI) m/z calculated for $C_{15}H_{19}BN_2O_2 + H^+$ [$M + H^+$]: 271.2. Found: 206.9 (consistent with hydrolysis of boronate ester).

6-Bromo-2-(fluoromethyl)benzo[d]thiazole (28a). Et_3N (4.4 mL, 31.6 mmol) was added dropwise to a suspension of 2-amino-5-bromobenzenethiol (**25**) (1.27 g, 6.24 mmol), PPh_3 (6.10 g, 23.3 mmol), and fluoroacetic acid (0.46 mL, 8.07 mmol) in CCl_4 (24 mL). The reaction mixture was heated at 95 °C for 1.5 h and was then allowed to cool to rt. The mixture was filtered through diatomaceous earth, washing with DCM. The filtrate was suspended in Et_2O , filtered, and the filtrate was concentrated and purified by silica gel chromatography, eluting with a gradient of 50–60% DCM/hexanes to give **28a** (318 mg, 21% yield) as a rust-colored powder. 1H NMR (400 MHz, $CDCl_3$): δ 8.09 (d, $J = 1.6$ Hz, 1H), 7.90 (d, $J = 8.8$ Hz, 1H), 7.63 (dd, $J = 8.6, 1.8$ Hz, 1H), 5.74 (d, $J = 48$ Hz, 2H). HPLC–MS (ESI) m/z calculated for $C_8H_7BrFNS + H^+$ [$M + H^+$]: 245.9/247.9. Found: 245.9/248.0.

6-Bromo-2-(difluoromethyl)benzo[d]thiazole (28b). Difluoroacetyl chloride (4.51 g, 39.4 mmol) was added dropwise to a solution of 2,2'-disulfanediybis(4-bromoaniline) (**26**) (2.00 g, 4.92 mmol) and pyridine (1.6 mL, 20 mmol) in DCM (20 mL). The mixture was stirred at rt for 2 h and was then concentrated and extracted into 3:1 EtOAc/MeOH (3 \times 20 mL) from water (25 mL). The combined organic extracts were dried (Na_2SO_4), filtered, and concentrated to give crude N,N' -(disulfanediybis(4-bromo-2,1-phenylene))bis(2,2-difluoroacetamide) (**27**) (2.77 g, 4.93 mmol), which was used without further purification. HPLC–MS (ESI) m/z calculated for $C_{16}H_{10}Br_2F_4N_2O_2S_2 + Na^+$ [$M + Na^+$]: 582.8/584.8/586.8. Found: 582.5/584.5/586.5.

A mixture of the crude **27** (2.77 g, 4.93 mmol) and dithiothreitol (3.80 g, 24.6 mmol) in DMF (8 mL) was stirred under inert atmosphere at rt for 16 h. The reaction mixture was diluted with water (120 mL) and the precipitate was collected by filtration, washing with water, to give **28b** (2.29 g, 88% yield) as a pale-yellow solid. 1H NMR (400 MHz, $CDCl_3$): δ 8.13 (dd, $J = 1.9, 0.4$ Hz, 1H), 7.98 (d, $J = 8.7$ Hz, 1H), 7.68 (dd, $J = 8.7, 2.0$ Hz, 1H), 6.92 (t, $J = 54$ Hz, 1H). ^{19}F NMR (377 MHz, $CDCl_3$): δ -110.59 (d, $J = 55$ Hz, 2F). ^{13}C NMR (100 MHz, $CDCl_3$): δ 162.38 (t, $J = 31$ Hz), 151.27, 136.50 (t, $J = 1$ Hz), 130.61, 125.53, 124.75, 120.80 (t, $J = 1$ Hz), 110.75 (t, $J = 240$ Hz). HPLC–MS (ESI) m/z calculated for $C_8H_4BrF_2NS + H^+$ [$M + H^+$]: 263.9/265.9. Found: 263.9/265.9.

6-Bromo-2-(trifluoromethyl)benzo[d]thiazole (28c). **28c** was acquired from commercial sources (Oxchem product list).

General Procedure for the Synthesis of Intermediates 29a–c. A suspension of an aryl bromide selected from **28a–c** (7.73 mmol), bis(pinacolato)diboron (1.50 equiv, 2.95 g, 11.6 mmol), $Pd(dppf)_2Cl_2 \cdot CH_2Cl_2$ (0.15 equiv, 0.95 g, 0.79 mmol), and KOAc (3.0 equiv, 2.28 g, 23.2 mmol) in 1,4-dioxane (25 mL) was heated in a microwave reactor at 120 °C for 30 min and then allowed to cool to rt. The reaction mixture was filtered through a pad of diatomaceous earth, washing with DCM and MeOH. The filtrate was concentrated and purified by silica gel chromatography, eluting with a gradient of 20–100% EtOAc/hexanes to give **29a–c**.

2-(Fluoromethyl)-6-(4,4,5,5-tetramethyl-1,3,2-dioxaborolan-2-yl)benzo[d]thiazole (29a). Tan solid, yield 100% (417 mg, 1.42 mmol). 1H NMR (400 MHz, $CDCl_3$): δ 8.43 (s, 1H), 8.05–8.01 (m, 1H), 7.93 (d, $J = 8.2$ Hz, 1H), 5.77 (d, $J = 44$ Hz, 2H), 1.39 (s, 12H). HPLC–MS (ESI) m/z calculated for $C_{14}H_{17}BFNO_2S + H^+$ [$M + H^+$]: 294.1. Found: 294.0.

2-(Difluoromethyl)-6-(4,4,5,5-tetramethyl-1,3,2-dioxaborolan-2-yl)benzo[d]thiazole (29b). Pale-yellow solid, yield 90% (2.16 g, 6.95 mmol). 1H NMR (400 MHz, $CDCl_3$): δ 8.47 (s, 1H), 8.12 (d, $J = 8.2$ Hz, 1H), 7.98 (d, $J = 8.2$ Hz, 1H), 6.95 (t, $J = 54$ Hz, 1H) 1.36 (s, 12H). HPLC–MS (ESI) m/z calculated for $C_{14}H_{16}BF_2NO_2S + H^+$ [$M + H^+$]: 312.1. Found: 311.9.

6-(4,4,5,5-Tetramethyl-1,3,2-dioxaborolan-2-yl)-2-(trifluoromethyl)benzo[d]thiazole (29c). Tan solid, yield 89% (0.461 g, 1.40 mmol). 1H NMR (400 MHz, $CDCl_3$): δ 8.47 (s, 1H), 8.18 (d, $J = 8.2$ Hz, 1H), 8.00 (s, 1H), 1.38 (s, 12H). HPLC–MS

(ESI) m/z calculated for $C_{14}H_{15}BF_3NO_2S + H^+$ [$M + H^+$]: 330.1. Found: 329.9.

General Procedure for the Synthesis of PERK Inhibitors 30–33, 37–40, and 42–44. Method A. A mixture of a 4-benzoyl-1H-pyrazol-3(2H)-one selected from **13b**, **13d**, **14a**, and **14c** (27.5 mmol), a boronate ester selected from **6**, **20–24**, **29a**, and **29c** (2.0 equiv, 55.0 mmol), and K_3PO_4 (3.0 equiv, 17.5 g, 82 mmol) in toluene (65 mL), MeOH (35 mL), and water (20 mL) was deoxygenated by bubbling argon through the mixture for 5 min. $Pd(PPh_3)_4$ (0.15 equiv, 4.76 g, 4.12 mmol) was added, and the reaction vessel was then sealed under an argon atmosphere and heated at 100 °C for 8 h. The mixture was allowed to cool to rt and was then diluted with 1:1 MeOH/DCM (200 mL) and filtered through a pad of diatomaceous earth. The filtrate was concentrated and purified by silica gel chromatography, eluting with a gradient of 0–6% 2 M NH_3 in MeOH/DCM to give the title compound.

Method B. A suspension of a 4-benzoyl-1H-pyrazol-3(2H)-one selected from **13b**, **13d**, **14a**, and **14c** (0.384 mmol), a boronate ester selected from **6**, **20–24**, **29a**, and **29c** (1.3 equiv, 0.507 mmol), bis(*di-tert-butyl*(4-dimethylaminophenyl)phosphine)dichloropalladium(II) (0.10 equiv, 27 mg, 0.038 mmol), and $Na_2CO_3 \cdot H_2O$ (3.0 equiv, 0.122 g, 1.15 mmol) in DMF (4 mL) and water (0.5 mL) was heated at 110 °C for 30 min. The reaction mixture was allowed to cool to rt and was then poured into water (30 mL). The resulting precipitate was collected by filtration, washed with water, and purified by silica gel chromatography, eluting with a gradient of 0–6% 2 M NH_3 in MeOH/DCM to give the title compound.

For those products isolated as HCl salts, the purified free base was dissolved in a 2:1 mixture of MeOH/DCM, and 1 N aqueous HCl (1.05 equiv) was added. The mixture was stirred for 45 min, filtered, concentrated, and dried. The residue was diluted with hexanes and sonicated to break up lumps. The solid was collected by filtration, washing with hexanes, to give the corresponding HCl salt.

General Procedure for the Synthesis of PERK Inhibitors 34–36 and 41. The 2-nitrobenzoyl-1H-pyrazol-3(2H)-one **13a** (3.04 g, 5.64 mmol), a boronate ester selected from **19a–c** and **29b** (2.5 equiv, 14.3 mmol), bis(*di-tert-butyl*(4-dimethylaminophenyl)phosphine)dichloropalladium(II) (0.10 equiv, 424 mg, 0.599 mmol), and $Na_2CO_3 \cdot H_2O$ (4.8 equiv, 2.86 g, 27.0 mmol) in DMF (40 mL) and water (4 mL) was heated at 110 °C for 30 min. The reaction mixture was allowed to cool to rt and was then poured into water (300 mL). The resulting precipitate was collected by filtration, washing with water. The solid was purified by silica gel chromatography, eluting with a gradient of 0–5% MeOH/DCM. The resulting nitro product was suspended in EtOH (60 mL) and AcOH (6 mL). Iron powder (11 equiv, 3.47 g, 62.1 mmol) was added, and the mixture was heated at 80 °C for 2.5 h. The reaction mixture was allowed to cool to rt and was filtered through a pad of diatomaceous earth, washing with MeOH, DCM, and 10:1 MeOH/AcOH. The filtrate was concentrated and treated with aqueous 5 N NaOH followed by saturated aqueous $NaHCO_3$ to raise the pH to 7. The suspension was filtered, and the solid was washed with water. The solid was purified by silica gel chromatography, eluting with a gradient of 0–6% 2 M NH_3 in MeOH/DCM to give **34–36** and **41**.

4-(2-Amino-4-methyl-3-(2-(methylamino)quinazolin-6-yl)-benzoyl)-1-methyl-2,5-diphenyl-1H-pyrazol-3(2H)-one (30). **30** was prepared by method B from **6** and **14a** as a rust-colored solid, yield 58% (121 mg, 0.22 mmol). 1H NMR (400 MHz, DMSO- d_6): δ 9.11 (s, 1H), 7.78 (d, $J = 8.2$ Hz, 1H), 7.53–7.67 (m, 11H), 7.35–7.50 (m, 3H), 6.59 (t, $J = 9.3$ Hz, 1H), 6.52 (br s, 2H), 3.12 (s, 3H), 2.94 (d, $J = 4.7$ Hz, 3H), 1.94–2.01 (m, 3H). ^{13}C NMR (100 MHz, DMSO- d_6): δ 190.5, 161.9, 161.4, 160.3, 157.8, 151.1, 149.0, 142.9, 136.2, 134.6, 133.8, 130.5, 129.7, 129.2, 129.2, 128.9, 128.1, 127.0, 126.5, 125.9, 124.6, 120.1, 116.8, 116.4, 111.2, 37.8, 28.1, 21.0. HRMS (ESI) m/z calculated for $C_{33}H_{28}N_6O_2 + H^+$ [$M + H^+$]: 541.2352. Found: 541.2350.

1-Methyl-4-(4-methyl-3-(2-(methylamino)quinazolin-6-yl)-benzoyl)-2,5-diphenyl-1H-pyrazol-3(2H)-one (31). **31** was prepared by method B from **6** and **13b** as an off-white solid, yield 43% (100 mg, 0.19 mmol). 1H NMR (400 MHz, DMSO- d_6): δ 9.15 (br s,

1H), 7.62–7.80 (m, 4H), 7.49–7.60 (m, 10H), 7.35–7.48 (m, 3H), 3.15 (s, 3H), 2.94 (d, *J* = 4.9 Hz, 3H), 2.32 (s, 3H). ¹³C NMR (100 MHz, DMSO-*d*₆): δ 187.8, 162.1, 161.6, 160.3, 158.2, 150.8, 140.2, 139.9, 135.9, 135.2, 134.2, 133.8, 130.8, 130.5, 130.3, 129.6, 129.2, 128.7, 128.3, 128.0, 127.8, 127.6, 125.4, 124.7, 119.3, 107.7, 37.1, 28.0, 20.4. HRMS (ESI) *m/z* calculated for C₃₃H₂₇N₅O₂ + H⁺ [M + H⁺]: 526.2243. Found: 526.2244.

4-(4-Amino-3-(2-(methylamino)quinazolin-6-yl)benzoyl)-1-methyl-2,5-diphenyl-1H-pyrazol-3(2H)-one (32). 32 was prepared by method B from 6 and 14c as a yellow solid, yield 37% (83 mg, 0.16 mmol). ¹H NMR (400 MHz, DMSO-*d*₆): δ 9.14 (br s, 1H), 7.73–7.83 (m, 1H), 7.50–7.68 (m, 13H), 7.33–7.48 (m, 2H), 6.77 (d, *J* = 8.4 Hz, 1H), 5.85 (br s, 2H), 3.09 (s, 3H), 2.94 (d, *J* = 4.7 Hz, 3H). ¹³C NMR (100 MHz, DMSO-*d*₆): δ 186.1, 162.2, 161.7, 160.1, 158.2, 150.8, 150.5, 135.1, 134.6, 133.1, 132.0, 130.9, 130.5, 129.4, 129.1, 128.8, 128.3, 127.5, 127.0, 126.0, 125.3, 124.7, 123.3, 119.6, 113.9, 109.8, 37.7, 28.1. HRMS (ESI) *m/z* calculated for C₃₂H₂₆N₆O₂ + H⁺ [M + H⁺]: 527.2196. Found: 527.2196.

4-(4-Chloro-3-(2-(methylamino)quinazolin-6-yl)benzoyl)-1-methyl-2,5-diphenyl-1H-pyrazol-3(2H)-one (33). 33 was prepared by method A from 6 and 13d as a pale-yellow solid, yield 46% (135 mg, 0.25 mmol). ¹H NMR (400 MHz, DMSO-*d*₆): δ 9.17 (br s, 1H), 7.85 (s, 2H), 7.73–7.82 (m, 2H), 7.44–7.66 (m, 13H), 3.17 (s, 3H), 2.95 (d, *J* = 4.7 Hz, 3H). ¹³C NMR (100 MHz, DMSO-*d*₆): δ 186.8, 162.2, 161.5, 160.4, 157.9, 151.2, 138.4, 137.3, 135.2, 135.1, 134.0, 132.3, 131.4, 130.5, 129.7, 129.7, 129.6, 129.2, 128.7, 128.4, 127.9, 127.8, 125.9, 124.6, 119.1, 106.6, 36.8, 28.0. HRMS (ESI) *m/z* calculated for C₃₂H₂₄ClN₅O₂ + H⁺ [M + H⁺]: 546.1697. Found: 546.1696.

4-(2-Amino-3-(5-fluoro-2-(methylamino)quinazolin-6-yl)-4-methylbenzoyl)-1-methyl-2,5-diphenyl-1H-pyrazol-3(2H)-one (34). 34 was prepared in two steps from 13a and 19a as a yellow solid, overall yield 35% (1.84 g, 3.29 mmol). ¹H NMR (400 MHz, DMSO-*d*₆): δ 9.28 (br s, 1H), 7.82 (d, *J* = 8.2 Hz, 1H), 7.41–7.65 (m, 13H), 6.68 (br s, 2H), 6.60 (d, *J* = 8.4 Hz, 1H), 3.13 (s, 3H), 2.94 (d, *J* = 4.9 Hz, 3H), 1.98 (s, 3H). ¹⁹F NMR (377 MHz, DMSO-*d*₆): δ -124.58 (s, 1F). ¹³C NMR (100 MHz, DMSO-*d*₆): δ 190.4, 161.3, 160.4, 157.9, 157.1, 155.7, 154.6, 152.9, 149.4, 143.8, 137.1, 134.5, 130.5, 129.2, 129.2, 128.9, 128.1, 127.1, 124.6, 122.1, 120.0, 116.6, 116.4, 114.1, 111.0, 110.2, 110.1, 37.7, 28.0, 20.6. HRMS (ESI) *m/z* calculated for C₃₃H₂₇N₅O₂ + H⁺ [M + H⁺]: 559.2258. Found: 559.2257.

4-(2-Amino-3-(5-chloro-2-(methylamino)quinazolin-6-yl)-4-methylbenzoyl)-1-methyl-2,5-diphenyl-1H-pyrazol-3(2H)-one (35). 35 was prepared in two steps from 13a and 19b as a yellow solid, overall yield 9% (54 mg, 0.094 mmol). ¹H NMR (400 MHz, DMSO-*d*₆): δ 9.35 (br s, 1H), 7.70–7.89 (m, 1H), 7.52–7.68 (m, 10H), 7.46 (d, *J* = 8.4 Hz, 3H), 6.59 (br s, 3H), 3.12 (br s, 3H), 2.96 (br s, 3H), 1.91 (br s, 3H). ¹³C NMR (100 MHz, DMSO-*d*₆): δ 190.4, 161.4, 160.4, 158.5, 157.8, 148.9, 143.2, 136.8, 134.5, 134.4, 131.7, 130.5, 129.2, 129.2, 129.2, 128.9, 128.5, 128.2, 127.1, 125.6, 124.6, 124.1, 117.5, 116.5, 116.4, 111.0, 37.7, 28.0, 20.3. HRMS (ESI) *m/z* calculated for C₃₃H₂₇ClN₅O₂ + H⁺ [M + H⁺]: 575.1962. Found: 575.1959.

4-(2-Amino-4-methyl-3-(2-methylquinazolin-6-yl)benzoyl)-1-methyl-2,5-diphenyl-1H-pyrazol-3(2H)-one (36). 36 was prepared in two steps from 13a and 19c as a yellow solid, overall yield 23% (57 mg, 0.11 mmol). ¹H NMR (400 MHz, DMSO-*d*₆): δ 9.53 (s, 1H), 7.95–8.08 (m, 2H), 7.82 (d, *J* = 8.2 Hz, 1H), 7.78 (d, *J* = 8.4 Hz, 1H), 7.52–7.65 (m, 10H), 6.49–6.69 (m, 3H), 3.13 (s, 3H), 2.82 (s, 3H), 1.96 (s, 3H). ¹³C NMR (100 MHz, DMSO-*d*₆): δ 190.5, 164.0, 161.4, 160.7, 157.9, 149.1, 148.9, 142.7, 136.8, 135.5, 134.5, 134.2, 130.5, 129.2, 129.2, 129.0, 128.9, 128.2, 128.1, 127.1, 126.0, 124.6, 123.3, 116.8, 116.5, 111.1, 37.8, 26.7, 20.9. HRMS (ESI) *m/z* calculated for C₃₃H₂₇N₅O₂ + H⁺ [M + H⁺]: 526.2243. Found: 526.2242.

4-(2-Amino-4-methyl-3-(2-methylbenzo[d]thiazol-5-yl)benzoyl)-1-methyl-2,5-diphenyl-1H-pyrazol-3(2H)-one (37). 37 was prepared by method A from 14a and 21 as a pale-yellow solid, yield 29% (45 mg, 0.085 mmol). ¹H NMR (400 MHz, DMSO-*d*₆): δ 8.17 (d, *J* = 8.2 Hz, 1H), 7.70–7.82 (m, 2H), 7.53–7.65 (m, 9H), 7.43 (t, *J* = 6.8 Hz, 1H), 7.21 (dd, *J* = 1.6, 8.2 Hz, 1H), 6.59 (d, *J* = 8.4 Hz,

1H), 6.45 (br s, 2H), 3.12 (s, 3H), 2.84 (s, 3H), 1.95 (s, 3H). ¹³C NMR (100 MHz, DMSO-*d*₆): δ 190.4, 167.5, 161.4, 157.8, 153.9, 148.9, 142.8, 134.5, 133.9, 130.5, 129.2, 129.2, 129.2, 128.9, 128.1, 127.1, 126.8, 126.6, 124.6, 123.2, 123.0, 116.8, 116.4, 111.2, 37.8, 21.0, 19.8. HRMS (ESI) *m/z* calculated for C₃₂H₂₆N₄O₂S + H⁺ [M + H⁺]: 531.1855. Found: 531.1856.

4-(2-Amino-4-methyl-3-(2-methylbenzo[d]thiazol-6-yl)benzoyl)-1-methyl-2,5-diphenyl-1H-pyrazol-3(2H)-one (38). 38 was prepared by method A from 14a and 22 as a tan solid, yield 61% (95 mg, 0.18 mmol). ¹H NMR (400 MHz, DMSO-*d*₆): δ 8.04 (d, *J* = 8.2 Hz, 1H), 7.90 (d, *J* = 1.4 Hz, 1H), 7.78 (d, *J* = 8.2 Hz, 1H), 7.51–7.65 (m, 9H), 7.38–7.48 (m, 1H), 7.28 (dd, *J* = 1.6, 8.2 Hz, 1H), 6.58 (d, *J* = 8.2 Hz, 1H), 6.46 (br s, 2H), 3.12 (s, 3H), 2.84 (s, 3H), 1.94 (s, 3H). ¹³C NMR (100 MHz, DMSO-*d*₆): δ 190.4, 167.3, 161.4, 157.8, 152.4, 148.9, 142.8, 136.2, 134.6, 133.9, 133.1, 130.5, 129.2, 129.2, 128.9, 128.1, 128.0, 127.0, 126.8, 124.6, 123.3, 122.7, 116.8, 116.4, 111.2, 37.8, 21.0, 19.8. HRMS (ESI) *m/z* calculated for C₃₂H₂₆N₄O₂S + H⁺ [M + H⁺]: 531.1855. Found: 531.1852.

4-(2-Amino-4-methyl-3-(2-(methylamino)benzo[d]thiazol-6-yl)benzoyl)-1-methyl-2,5-diphenyl-1H-pyrazol-3(2H)-one (39). 39 was prepared by method A from 14a and 23 as a pale-yellow solid, yield 56% (1.12 g, 2.05 mmol). ¹H NMR (400 MHz, DMSO-*d*₆): δ 10.13 (br s, 1H), 7.77 (d, *J* = 8.2 Hz, 1H), 7.71 (s, 1H), 7.67–7.71 (m, 1H), 7.53–7.64 (m, 9H), 7.43 (t, *J* = 6.8 Hz, 1H), 7.22 (dd, *J* = 1.6, 8.2 Hz, 1H), 6.58 (d, *J* = 8.4 Hz, 1H), 4.43 (br s, 2H), 3.15 (s, 3H), 3.12 (s, 3H), 1.94 (s, 3H). ¹³C NMR (100 MHz, DMSO-*d*₆): δ 190.4, 167.7, 161.3, 157.8, 148.8, 142.8, 134.5, 133.9, 131.6, 130.5, 129.2, 129.2, 129.2, 128.9, 128.8, 128.1, 127.1, 126.6, 124.6, 123.9, 116.8, 116.5, 116.1, 111.1, 37.8, 31.7, 20.9. HRMS (ESI) *m/z* calculated for C₃₂H₂₇N₅O₂S + H⁺ [M + H⁺]: 546.1964. Found: 546.1964.

4-(2-Amino-3-(2-aminobenzo[d]thiazol-6-yl)-4-methylbenzoyl)-1-methyl-2,5-diphenyl-1H-pyrazol-3(2H)-one Hydrochloride (40). 40 was prepared by method A from 14a and 24 as a yellow solid, yield 28% (90 mg, 0.17 mmol). Note: Deacetylation of the *N*-acetyl-2-aminobenzothiazole occurred under the reaction conditions. ¹H NMR (400 MHz, DMSO-*d*₆): δ 9.95 (br s, 2H), 7.76 (s, 1H), 7.77 (d, *J* = 10.0 Hz, 2H), 7.52–7.69 (m, 9H), 7.40–7.47 (m, 1H), 7.26 (dd, *J* = 1.6, 8.4 Hz, 1H), 6.58 (d, *J* = 8.4 Hz, 1H), 4.72 (br s, 3H), 3.12 (s, 3H), 1.93 (s, 3H). ¹³C NMR (100 MHz, DMSO-*d*₆): δ 190.4, 169.0, 161.3, 157.8, 148.7, 142.8, 138.8, 134.5, 134.0, 132.4, 130.5, 129.3, 129.2, 129.2, 128.9, 128.1, 127.1, 126.4, 125.3, 124.6, 124.5, 116.8, 116.5, 115.2, 111.0, 37.7, 20.9. HRMS (ESI) *m/z* calculated for C₃₁H₂₅N₅O₂S + H⁺ [M + H⁺]: 532.1807. Found: 532.1805.

4-(2-Amino-3-(2-(fluoromethyl)benzo[d]thiazol-6-yl)-4-methylbenzoyl)-1-methyl-2,5-diphenyl-1H-pyrazol-3(2H)-one (41). 41 was prepared in two steps from 13a and 29a as a yellow solid, overall yield 14% (42 mg, 0.077 mmol). ¹H NMR (400 MHz, DMSO-*d*₆): δ 8.19 (d, *J* = 8.4 Hz, 1H), 8.06 (s, 1H), 7.80 (d, *J* = 8.2 Hz, 1H), 7.52–7.65 (m, 9H), 7.43 (t, *J* = 6.9 Hz, 1H), 7.38 (d, *J* = 8.6 Hz, 1H), 6.60 (d, *J* = 8.4 Hz, 1H), 6.49 (br s, 2H), 5.92 (d, *J* = 45 Hz, 2H), 3.12 (s, 3H), 1.95 (s, 3H). ¹⁹F NMR (377 MHz, DMSO-*d*₆): δ -73.40 (s, 1F). ¹³C NMR (100 MHz, DMSO-*d*₆): δ 190.4, 166.1 (d, *J* = 23 Hz), 161.4, 157.8, 151.9, 148.9, 142.8, 135.7, 134.5, 134.3, 134.0, 130.5, 129.2, 129.2, 128.9, 128.7, 128.1, 127.1, 126.6, 124.6, 124.0, 123.9, 116.8, 116.5, 111.2, 81.2 (d, *J* = 165 Hz), 37.8, 21.0. HRMS (ESI) *m/z* calculated for C₃₂H₂₅FN₄O₂S + H⁺ [M + H⁺]: 549.1761. Found: 549.1760.

4-(2-Amino-3-(2-(difluoromethyl)benzo[d]thiazol-6-yl)-4-methylbenzoyl)-1-methyl-2,5-diphenyl-1H-pyrazol-3(2H)-one (42). 42 was prepared by method A from 14a and 29b as a tan solid, yield 57% (1.55 g, 2.73 mmol). ¹H NMR (400 MHz, DMSO-*d*₆): δ 8.34 (d, *J* = 8.4 Hz, 1H), 8.20 (d, *J* = 1.2 Hz, 1H), 7.85 (d, *J* = 8.2 Hz, 1H), 7.57–7.73 (m, 10H), 7.44–7.52 (m, 2H), 6.65 (d, *J* = 8.4 Hz, 1H), 3.87–5.89 (br s, 2H), 3.17 (s, 3H), 1.99 (s, 3H). ¹⁹F NMR (377 MHz, DMSO-*d*₆): δ -110.82 (d, *J* = 41 Hz, 2F). ¹³C NMR (100 MHz, DMSO-*d*₆): δ 190.4, 162.1 (t, *J* = 30 Hz), 161.3, 157.8, 151.4, 148.8, 142.7, 135.6, 135.2, 134.5, 134.1, 130.5, 129.5, 129.2, 129.2, 129.2, 129.2, 128.9, 128.1, 127.1, 126.4, 124.8, 124.6, 116.8, 116.6, 109.9 (t, *J*

= 239 Hz), 37.8, 20.9. HRMS (ESI) m/z calculated for $C_{32}H_{24}F_2N_4O_2S + H^+$ [M + H⁺]: 567.1666. Found: 567.1667.

4-(2-Amino-4-methyl-3-(2-(trifluoromethyl)benzo[d]thiazol-6-yl)benzoyl)-1-methyl-2,5-diphenyl-1H-pyrazol-3(2H)-one (43). 43 was prepared by method A from 14a and 29c as a pale-yellow solid, yield 46% (95 mg, 0.16 mmol). ¹H NMR (400 MHz, DMSO-*d*₆): δ 8.40 (d, *J* = 8.4 Hz, 1H), 8.24 (d, *J* = 1.2 Hz, 1H), 7.82 (d, *J* = 8.2 Hz, 1H), 7.52–7.64 (m, 10H), 7.43 (t, *J* = 6.8 Hz, 1H), 6.61 (d, *J* = 8.2 Hz, 1H), 6.54 (br s, 2H), 3.13 (s, 3H), 1.95 (s, 3H). ¹⁹F NMR (377 MHz, DMSO-*d*₆): δ -60.72 (s, 1F). ¹³C NMR (100 MHz, DMSO-*d*₆): δ 190.4, 161.3, 157.9, 155.1 (q, *J* = 40 Hz), 151.0, 148.8, 142.6, 136.7, 135.7, 134.5, 134.3, 130.5, 130.2, 129.2, 129.2, 128.9, 128.1, 127.1, 126.1, 125.4, 124.9, 124.6, 119.8 (q, *J* = 273 Hz), 116.8, 116.5, 111.1, 37.7, 20.9. HRMS (ESI) m/z calculated for $C_{32}H_{23}F_3N_4O_2S + H^+$ [M + H⁺]: 585.1572. Found: 585.1576.

4-(2-Amino-4-methyl-3-(2-methylquinolin-6-yl)benzoyl)-1-methyl-2,5-diphenyl-1H-pyrazol-3(2H)-one Hydrochloride (44). 44 was prepared by method A from 14a and 20 (Aldrich) as a pale-yellow solid, yield 54% (8.38 g, 14.9 mmol). ¹H NMR (400 MHz, DMSO-*d*₆): δ 9.03 (d, *J* = 8.6 Hz, 1H), 8.60 (d, *J* = 8.8 Hz, 1H), 8.21 (d, *J* = 1.4 Hz, 1H), 7.99 (d, *J* = 8.8 Hz, 1H), 7.95 (d, *J* = 8.8 Hz, 1H), 7.85 (d, *J* = 8.2 Hz, 1H), 7.53–7.65 (m, 9H), 7.43 (t, *J* = 6.8 Hz, 1H), 6.64 (d, *J* = 8.4 Hz, 1H), 3.73 (br s, 3H), 3.14 (s, 3H), 3.05 (s, 3H), 1.95 (s, 3H). ¹³C NMR (100 MHz, DMSO-*d*₆): δ 190.5, 161.3, 157.9, 157.7, 148.6, 144.9, 142.6, 137.4, 136.5, 134.5, 134.5, 130.6, 130.4, 129.2, 129.2, 129.2, 128.9, 128.1, 127.6, 127.1, 125.4, 124.7, 123.8, 121.5, 117.0, 116.7, 110.9, 37.7, 20.9, 20.4. HRMS (ESI) m/z calculated for $C_{34}H_{28}N_4O_2 + H^+$ [M + H⁺]: 525.2291. Found: 525.2290.

1-(5-Bromoindolin-1-yl)-2-(3-fluoro-5-(trifluoromethyl)phenyl)ethanone (47). A suspension of 2-(3-fluoro-5-(trifluoromethyl)phenyl)acetic acid (45) (25.45 g, 115 mmol) in THF (200 mL) was treated with 1,1'-carbonyldiimidazole (17.77 g, 110 mmol), and the mixture was stirred at rt for 10 min (until a clear solution was obtained and the initial effervescence subsided). The solution was then heated at 60 °C for 2 h, after which time effervescence had ceased. The solution was allowed to cool to rt, and 5-bromoindoline (46) (19.73 g, 100 mmol) was added. The resulting solution was stirred for 20 h. The solution was concentrated, dissolved in EtOAc (400 mL), and washed with 2 N aqueous HCl (2 × 200 mL) followed by saturated aqueous NaHCO₃ (2 × 200 mL). The EtOAc extract was dried (MgSO₄), filtered, concentrated, and recrystallized by dissolving in EtOAc (100 mL), diluting with hexanes (400 mL), and allowing it to stand at -20 °C for 16 h. The resulting white solid was collected by filtration, washing with hexanes, to give 47 (33.65 g, 84% yield) as a white crystalline solid. ¹H NMR (400 MHz, DMSO-*d*₆): δ 7.95 (d, *J* = 8.0 Hz, 1H), 7.43–7.59 (m, 4H), 7.32 (d, *J* = 8.2 Hz, 1H), 4.23 (t, *J* = 7.5 Hz, 2H), 4.03 (br s, 2H), 3.15–3.27 (m, 2H). HPLC-MS (ESI) m/z calculated for $C_{17}H_{12}BrF_4NO + H^+$ [M + H⁺]: 402.0/404.0. Found: 402.0/404.0.

2-(3-Fluoro-5-(trifluoromethyl)phenyl)-1-(5-(4,4,5,5-tetra-methyl-1,3,2-dioxaborolan-2-yl)indolin-1-yl)ethanone (48). A mixture of 47 (33.49 g, 83 mmol), bis(pinacolato)diboron (44.4 g, 175 mmol), KOAc (24.52 g, 250 mmol), and Pd(dppf)Cl₂·DCM (3.01 g, 3.69 mmol) in 1,4-dioxane (400 mL) was degassed by bubbling argon through the mixture for 30 min, and the mixture was then heated at 90 °C for 16 h. The mixture was allowed to cool, concentrated, dissolved in DCM (400 mL), and purified by silica gel chromatography, eluting with DCM to give a white solid. The solid was suspended in Et₂O (50 mL), stirred for 30 min, diluted with hexanes (300 mL), and concentrated to remove the Et₂O. The suspension was refrigerated in a -20 °C freezer for 1 h. The resulting white solid was collected by filtration, washing with hexanes, to give 48 (32.91 g, 88% yield) as a fluffy white solid. ¹H NMR (400 MHz, DMSO-*d*₆): δ 7.88–8.13 (m, 1H), 7.39–7.64 (m, 5H), 4.22 (br s, 2H), 4.05 (br s, 2H), 3.19 (br s, 2H), 1.28 (s, 12H). HPLC-MS (ESI) m/z calculated for $C_{23}H_{24}BF_4NO_3 + H^+$ [M + H⁺]: 450.2. Found: 450.2.

4-Chloro-5-iodo-2,7-dimethyl-7H-pyrrolo[2,3-*d*]pyrimidine (50). A solution of 4-chloro-5-iodo-2-methyl-7H-pyrrolo[2,3-*d*]pyrimidine (49; Aurum PharmaTech) (8.63 g, 29.4 mmol) in DMF

(140 mL) was cooled in an ice-water bath, and NaH (60% in mineral oil; 1.53 g, 38.2 mmol) was added portionwise over 20 min. The mixture was stirred for an additional 2 h, and then iodomethane (2.0 mL, 32 mmol) was slowly added. The ice-water bath was removed, and the mixture was stirred for 16 h. The mixture was poured onto ice-water (600 mL) and stirred for 20 min. The precipitate was collected by filtration, washing with water, to give 50 (7.04 g, 78% yield) as a tan solid. ¹H NMR (400 MHz, DMSO-*d*₆): δ 7.88 (s, 1H), 3.79 (s, 3H), 2.66 (s, 3H). HPLC-MS (ESI) m/z calculated for $C_8H_7ClIN_3 + H^+$ [M + H⁺]: 307.9. Found: 307.9.

5-Iodo-2,7-dimethyl-7H-pyrrolo[2,3-*d*]pyrimidin-4-amine (51). A mixture of 50 (1.76 g, 5.72 mmol), concentrated aqueous NH₃ (20 mL, 515 mmol), and 1,4-dioxane (10 mL) was heated in a microwave reactor at 135 °C for 2 h. The mixture was allowed to cool to rt and the precipitate was collected by filtration, washing with water, to give 51 (1.28 g, 78% yield) as a tan solid. ¹H NMR (400 MHz, DMSO-*d*₆): δ 7.33 (s, 1H), 3.65 (s, 3H), 2.39 (s, 3H). HPLC-MS (ESI) m/z calculated for $C_8H_9IN_4 + H^+$ [M + H⁺]: 289.0. Found: 288.8.

1-(5-(4-Amino-2,7-dimethyl-7H-pyrrolo[2,3-*d*]pyrimidin-5-yl)indolin-1-yl)-2-(3-fluoro-5-(trifluoromethyl)phenyl)ethanone (52). A mixture of 48 (1.50 g, 3.34 mmol), 51 (0.874 g, 3.03 mmol), and K₃PO₄ (1.93 g, 9.10 mmol) in toluene (20 mL), MeOH (10 mL), and water (5 mL) was treated with Pd(PPh₃)₄ (350 mg, 0.30 mmol) and sealed under argon. The mixture was heated in a microwave reactor at 110 °C for 20 min. The reaction mixture was allowed to cool to rt and was diluted with 50% MeOH/DCM and filtered through a pad of diatomaceous earth. The filtrate was concentrated and purified by silica gel chromatography, eluting with a gradient of 0–100% EtOAc/DCM followed by 0–12% 2 M NH₃ in MeOH/DCM. The resulting product was slurried in EtOAc (50 mL) for 1 h, and the solid was collected by filtration to give 52 (0.592 g, 40% yield) as a white solid. ¹H NMR (400 MHz, DMSO-*d*₆): δ 8.11 (d, *J* = 8.2 Hz, 1H), 7.56–7.62 (m, 2H), 7.52 (d, *J* = 9.6 Hz, 1H), 7.32 (s, 1H), 7.23 (d, *J* = 8.2 Hz, 1H), 7.16 (s, 1H), 5.98 (br s, 2H), 4.27 (t, *J* = 8.4 Hz, 2H), 4.07 (s, 2H), 3.70 (s, 3H), 3.26 (t, *J* = 8.2 Hz, 2H), 2.43 (s, 3H). ¹⁹F NMR (377 MHz, DMSO-*d*₆): δ -61.06 (s, 3F), -111.73 (s, 1F). ¹³C NMR (100 MHz, DMSO-*d*₆): δ 168.0, 161.7 (d, *J* = 246 Hz), 159.9, 157.0, 151.4, 141.6, 140.0, 132.8, 130.5 (dq, *J* = 8, 33 Hz), 130.2, 127.0, 124.8 (q, *J* = 274 Hz), 124.7, 123.3, 123.0, 121.2, 116.2, 114.8, 110.8, 97.8, 47.8, 40.8, 30.6, 27.5, 25.4. HRMS (ESI) m/z calculated for $C_{25}H_{21}F_4N_5O + H^+$ [M + H⁺]: 484.1761. Found: 484.1763.

Purification of PERK Protein for Structural Studies. Human PERK (575-1094 Δ670-874) harboring the inactivating D937N mutation was expressed in *E. coli* BL21(DE3) cells as a His6-GST-fusion. Purification of the unphosphorylated protein was performed using glutathione Sepharose, TEV protease cleavage of the His6-GST tag, and SEC purification using a Superdex 75 column. Final purification buffer was 25 mM Tris, pH 7.5, 300 mM NaCl, 10 mM 2-mercaptoethanol, and 10% glycerol. Aliquots of PERK protein were buffer exchanged into 10 mM HEPES, pH 7.5, 300 mM NaCl, and 5 mM dithiothreitol, and the solution was then concentrated to ~8–10 mg/mL. Protein was mixed with 3 mol equiv of inhibitors from DMSO stock solutions and incubated on ice for 1 h prior to setting up crystallization trials.

Cocrystallization of 10b with PERK. Crystals of PERK with compound 10b were obtained at 4 °C in hanging drops with 100 mM BTP, pH 6.5, 300 mM Na₂SO₄, 14% PEG-3350. Mother liquor supplemented with ethylene glycol was used as cryoprotectant. Diffraction data for 10b with PERK were collected on beamline 5.0.2 at the Advanced Light Source (ALS) and processed and scaled with HKL 2000. The cocrystal structure was solved by molecular replacement using the structure of GCN2 (PDB code 1ZY4) as the template. Model building was carried out with Coot, and refinement was done using Refmac5.

Cocrystallization of 7 with PERK. Crystals of PERK with compound 7 were obtained at 4 °C in hanging drops with 0.6 M Na/K tartrate. Mother liquor supplemented with glycerol was used as cryoprotectant. Diffraction data for 7 with PERK were collected on

beamline 22-ID at the Advanced Photon Source (APS) and processed and scaled with HKL 2000. The cocrystal structure was solved using the structure of compound **10b** bound to PERK as the initial template. Model building was carried out with Coot, and refinement was done using Refmac5.

Cocrystallization of 34 with PERK. Crystals of PERK with compound **34** were obtained at 4 °C in hanging drops with 100 mM HEPES, pH 7.0, 180 mM Na/K tartrate, 5% PEG-3350. Mother liquor supplemented with glycerol was used as cryoprotectant. Diffraction data for **34** with PERK were collected on beamline 5.0.1 at the Advanced Light Source (ALS) and processed and scaled with HKL 2000. The cocrystal structure was solved using the structure of compound **7** bound to PERK as the initial template. Model building was carried out with Coot, and refinement was done using Refmac5.

Cocrystallization of 39 with PERK. Crystals of PERK with compound **39** were obtained at 4 °C in hanging drops with 100 mM MES, pH 6.5, 180 mM Na/K tartrate. Mother liquor supplemented with glycerol was used as cryoprotectant. Diffraction data for **39** with PERK were collected on beamline 5.0.1 at the Advanced Light Source (ALS) and processed and scaled with HKL 2000. The cocrystal structure was solved using the structure of compound **7** bound to PERK as the initial template. Model building was carried out with Coot, and refinement was done using Refmac5.

Cocrystallization of 44 with PERK. Crystals of PERK with compound **44** were obtained at 4 °C in hanging drops with 100 mM HEPES, pH 7.0, 400 mM Na/K tartrate. Mother liquor supplemented with glycerol was used as cryoprotectant. Diffraction data for **44** with PERK were collected on a Rigaku FR-E home source X-ray generator equipped with an R-Axis4 detector and processed and scaled with HKL 2000. The cocrystal structure was solved using the structure of compound **7** bound to PERK as the initial template. Model building was carried out with Coot, and refinement was done using Refmac5.

Cocrystallization of 52 with PERK. Crystals of PERK with compound **52** were obtained at 4 °C in hanging drops with 100 mM MES, pH 6.5, 150 mM NaCl, 12% PEG-3350. Mother liquor supplemented with ethylene glycol was used as cryoprotectant. Diffraction data for **52** with PERK were collected on beamline 5.0.2 at the Advanced Light Source (ALS) and processed and scaled with HKL 2000. The cocrystal structure was solved using the structure of compound **7** bound to PERK as the initial template. Model building was carried out with Coot, and refinement was done using Refmac5.

PERK and GCN2 Enzyme Assays. Human PERK and GCN2 enzyme assays were performed using TR-FRET assays (Cisbio Inc.) in an analogous manner to previously described LanthaScreen TR-FRET assays.³⁰ N-Terminal His-tagged PERK and C-terminal His-tagged GCN2 proteins were expressed in *E. coli*. His-tagged PERK was used at 1 nM concentration in the presence of 1 μM ATP (K_m concentration), and His-tagged GCN2 was used at 10 nM concentration in the presence of 120 μM ATP ($0.66 \times K_m$ concentration). The assay substrate was eIF2α (AviTag C-terminal, His N-terminal; eIF2α(3-315)) at 37.5 nM concentration.

Cell Culture. HT1080–T-REX–PERK–FLAG cells (Amgen) were grown in DMEM (Gibco) supplemented with 10% tetracycline-free FBS (Hyclone), 1× NEAA (Gibco), 5 μg/mL blasticidin (Invitrogen), and 400 μg/mL Zeocin (Invitrogen). HT1080 cells (ATCC) were grown in DMEM supplemented with 10% FBS (Gibco) and 1× NEAA. U2OS cells (ATCC) were grown in McCoy's 5A (Gibco) supplemented with 10% FBS, 1× PSG (Gibco), and 1× NEAA. All cells were grown at 37 °C in the presence of 5% CO₂.

pPERK ELISA Assay. HT1080–T-REX–PERK–FLAG cells were seeded at 3×10^4 cells/mL in 96-well flat-bottomed plates (Corning) and incubated overnight. PERK was overexpressed by addition of 25 ng/mL doxycycline (Sigma) for 4 h. Then PERK inhibitor dose responses were added for 1 h. Cells were lysed in mPER (Pierce). pPERK sandwich ELISA was performed using FLAG antibody (Sigma) for total PERK capture and internally generated pPERK (T980) antibody for pPERK detection.

Protein Synthesis Rescue Assay. U2OS cells were seeded at 1×10^4 cells/mL in 96-well view-plates (PerkinElmer) and incubated overnight. Cells were dosed with PERK inhibitor dose responses for 1

h followed by the addition of 100 nM thapsigargin (Sigma) for 30 min to activate the PERK pathway. Newly synthesized protein was then quantified over a 30 min window using the Click-iT AHA AlexaFluor 488 protein synthesis HCS assay kit (Life Technologies).

PERK CHO_P Assay. HT1080 cells were seeded at 2×10^4 cells/mL in 96-well flat-bottomed plates (Corning) and incubated overnight. Cells were dosed with PERK inhibitor dose responses for 1 h followed by the addition of 100 nM thapsigargin for 2 h to induce CHO_P. Cells were lysed in bDNA lysis buffer (Affymetrix) containing 0.17 μg/mL final concentration of proteinase K (Affymetrix). CHO_P and GAPDH mRNA levels were quantified with the Quantigene 2.0 bDNA assay kit³¹ (Affymetrix). CHO_P mRNA was normalized to GAPDH mRNA.

pGCN2 MSD Assay. U2OS cells were seeded at 4×10^4 cells/mL in 96-well flat-bottomed plates (Corning) and incubated for 24 h. Cells were dosed with PERK inhibitor dose responses for 1 h. Cells were then washed with DMEM lacking arginine, leucine, and lysine (Sigma) followed by a 2 h incubation with PERK inhibitor dose responses in DMEM lacking arginine, leucine, and lysine to activate GCN2. Cells were then lysed in mPER. High binding plates (MSD) were then coated with 3 μL of lysate and incubated overnight at 4 °C. Plates were blocked with 5% blocker A (MSD) for 2.5 h at rt with shaking. Antibodies to either phospho-GCN2 (EpiTomics) or total-GCN2 (Cell Signaling) were added for 1 h at rt with shaking. Sulfo-Tag Goat anti-rabbit (MSD) was then added for 1 h at room temperature with shaking. Read buffer (MSD) was then added, and phospho and total GCN2 protein levels were quantified on a SECTOR Imager 6000 plate reader (MSD).

GCN2 CHO_P Assay. The same conditions were used as for the PERK CHO_P assay except cells were dosed with PERK inhibitor dose responses for 1 h followed by a 2 h incubation with PERK inhibitor dose responses in DMEM lacking arginine, leucine, and lysine to activate GCN2. Thapsigargin was omitted.

In Vivo PD Assay. Four- to six-week old naive athymic nude mice (Harlan Laboratories) were treated on day zero with 0.1 mg/mL doxycycline (Dox) H₂O supplied in drinking water ad libitum overnight. On day 1 of study, HT1080–T-REX–PERK–FLAG cells (cultured in DMEM + 10% FBS) were trypsinized and counted. All cells were suspended in 100% growth factor reduced Matrigel. Animals ($n = 3/\text{group}$) were first treated orally with a single dose of control or compound(s), and then Matrigel plugs containing 5×10^6 HT1080–T-REX–PERK–FLAG cells in 500 μL of Matrigel were injected subcutaneously into the animals' right flanks. Mice were euthanized with CO₂ asphyxiation, and plug samples were harvested 4 h after implantation and snap frozen in liquid nitrogen for analysis of PERK phosphorylation. Plasma samples were also taken for pharmacokinetic analysis. Tumor cell lysates were prepared by homogenization of the plugs in ice-cold radioimmunoprecipitation assay buffer [50 mmol/L Tris (pH 7.5), 150 mmol/L NaCl, 1% NP40, 0.5% sodium deoxycholate, and 0.1% SDS] containing protease and phosphatase inhibitors (Sigma) and assayed by pPERK sandwich ELISA using FLAG antibody (Sigma) for total PERK capture and internally generated pPERK antibody for pPERK detection.

Animal Use Policies. All animals used in the generation of data included in this manuscript were housed according to all Association for Assessment and Accreditation of Laboratory Animal Care specifications. Experimental procedures were done in accordance with Institutional Animal Care and Use Committee and United States Department of Agriculture regulations.

■ ASSOCIATED CONTENT

📄 Supporting Information

KINOMEScan kinase selectivity data for compounds **1**, **7**, **10b**, **30–36**, **38–44**, and **52**; X-ray crystallographic data for compounds **7**, **10b**, **34**, **39**, **44**, and **52** bound to PERK. This material is available free of charge via the Internet at <http://pubs.acs.org>.

Accession Codes

PDB codes for PERK with bound inhibitors: 7, 4X7J; 10b, 4X7H; 34, 4X7K; 39, 4X7L; 44, 4X7N; 52, 4X7O.

AUTHOR INFORMATION

Corresponding Authors

*A.L.S.: e-mail, adriansmith@roadrunner.com; phone, (805) 530-2367.

*J.R.L.: e-mail, jliford@amgen.com; phone, (805) 447-2140.

Notes

The authors declare no competing financial interest.

ACKNOWLEDGMENTS

The contributions of Nick Paras and Jeffrey Petkus are acknowledged for the original synthesis of compound 7. Josette Carnahan, Carol Babij, and Manory Fernando are thanked for obtaining B-Raf assay data on compounds. Andrew Tasker is thanked for useful discussions leading to the design of 34 and 35.

ABBREVIATIONS USED

ATF4, activating transcription factor 4; ATF6, activating transcription factor 6; BTP, Bis-Tris propane; CDI, 1,1'-carbonyldiimidazole; CHoP, C/EBP homologous protein; eIF2 α , eukaryotic initiation factor 2 α ; ELISA, enzyme-linked immunosorbent assay; ER, endoplasmic reticulum; GCN2, general control nonderepressible 2; GST, glutathione S-transferase; HATU, [dimethylamino(triazolo[4,5-*b*]pyridin-3-yloxy)methylidene]dimethylazanium hexafluorophosphate; HEPES, 4-(2-hydroxyethyl)-1-piperazineethanesulfonic acid; HRI, heme-regulated eIF2 α kinase; IRE-1, inositol-requiring enzyme 1; MES, 2-(*N*-morpholino)ethanesulfonic acid; MSD, Meso Scale Discovery; PD, pharmacodynamic; PERK, protein kinase R-like endoplasmic reticulum kinase; PKR, protein kinase RNA-activated; pGCN2, phospho-GCN2; pPERK, phospho-PERK; SAR, structure-activity relationship; TBTU, *O*-(benzotriazol-1-yl)-*N,N,N',N'*-tetramethyluronium tetrafluoroborate; UPR, unfolded protein response

REFERENCES

- (1) Ron, D.; Walter, P. Signal integration in the endoplasmic reticulum unfolded protein response. *Nat. Rev. Mol. Cell Biol.* **2007**, *8*, 519–529.
- (2) Shore, G. C.; Papa, F. R.; Oakes, S. A. Signaling cell death from the endoplasmic reticulum stress response. *Curr. Opin. Cell Biol.* **2011**, *23*, 143–149.
- (3) Carrara, M.; Prischi, F.; Ali, M. M. U. UPR signal activation by luminal sensor domains. *Int. J. Mol. Sci.* **2013**, *14*, 6454–6466.
- (4) Ma, Y.; Hendershot, L. M. The role of the unfolded protein response in tumor development: friend or foe? *Nat. Rev. Cancer* **2004**, *4*, 966–977.
- (5) Walter, P.; Ron, D. The unfolded protein response: from stress pathway to homeostatic regulation. *Science* **2011**, *334*, 1081–1086.
- (6) Vandewynckel, Y.-P.; Laukens, D.; Geerts, A.; Bogaerts, E.; Paridaens, A.; Verhelst, X.; Janssens, S.; Heindryckx, F.; van Vlierberghe, H. The paradox of the unfolded protein response in cancer. *Anticancer Res.* **2013**, *33*, 4683–4694.
- (7) Gao, Y.; Sartori, D. J.; Li, C.; Yu, Q.-C.; Kushner, J. A.; Simon, M. C.; Diehl, J. A. PERK is required in the adult pancreas and is essential for maintenance of glucose homeostasis. *Mol. Cell. Biol.* **2012**, *32*, 5129–5139.
- (8) Bi, M.; Naczki, C.; Koritzinsky, M.; Fels, D.; Blais, J.; Hu, N.; Harding, H.; Novoa, I.; Varia, M.; Raleigh, J.; Scheuner, D.; Kaufman, R. J.; Bell, J.; Ron, D.; Wouters, B. G.; Koumenis, C. ER stress-

regulated translation increases tolerance to extreme hypoxia and promotes tumor growth. *EMBO J.* **2005**, *24*, 3470–3481.

(9) Kim, I.; Xu, W.; Reed, J. C. Cell death and endoplasmic reticulum stress: disease relevance and therapeutic opportunities. *Nat. Rev. Drug Discovery* **2008**, *7*, 1013–1030.

(10) Fels, D. R.; Koumenis, C. The PERK/eIF2 α /ATF4 module of the UPR in hypoxia resistance and tumor growth. *Cancer Biol. Ther.* **2006**, *5*, 723–728.

(11) Wang, M.; Kaufman, R. J. The impact of the endoplasmic reticulum protein-folding environment on cancer development. *Nat. Rev. Cancer* **2014**, *14*, 581–597.

(12) Axten, J. M.; Medina, J. R.; Feng, Y.; Shu, A.; Romeril, S. P.; Grant, S. W.; Li, W. H. H.; Heerding, D. A.; Minthorn, E.; Mencken, T.; Atkins, C.; Liu, Q.; Rabindran, S.; Kumar, R.; Hong, X.; Goetz, A.; Stanley, T.; Taylor, J. D.; Sigethy, S. D.; Tomberlin, G. H.; Hassell, A. M.; Kahler, K. M.; Shewchuk, L. M.; Gampe, R. T. Discovery of 7-methyl-5-(1-{[3-(trifluoromethyl)phenyl]acetyl}-2,3-dihydro-1*H*-indol-5-yl)-7*H*-pyrrolo[2,3-*d*]pyrimidin-4-amine (GSK2606414), a potent and selective first-in-class inhibitor of protein kinase R (PKR)-like endoplasmic reticulum kinase (PERK). *J. Med. Chem.* **2012**, *55*, 7193–7207.

(13) Axten, J. M.; Romeril, S. P.; Shu, A.; Ralph, J.; Medina, J. R.; Feng, Y.; Li, W. H. H.; Grant, S. W.; Heerding, D. A.; Minthorn, E.; Mencken, T.; Gaul, N.; Goetz, A.; Stanley, T.; Hassell, A. M.; Gampe, R. T.; Atkins, C.; Kumar, R. Discovery of GSK2656157: an optimized PERK inhibitor selected for preclinical development. *ACS Med. Chem. Lett.* **2013**, *4*, 964–968.

(14) Smith, A. L.; DeMorin, F. F.; Paras, N. A.; Huang, Q.; Petkus, J. K.; Doherty, E. M.; Nixey, T.; Kim, J. L.; Whittington, D. A.; Epstein, L. F.; Lee, M. R.; Rose, M. J.; Babij, C.; Fernando, M.; Hess, K.; Le, Q.; Beltran, P.; Carnahan, J. Selective inhibitors of the mutant B-Raf pathway: discovery of a potent and orally bioavailable aminoisoquinoline. *J. Med. Chem.* **2009**, *52*, 6189–6192.

(15) Suzuki, A. Carbon-carbon bonding made easy. *Chem. Commun.* **2005**, 4759–4763.

(16) Liu, L.; Norman, M. H.; Lee, M.; Xi, N.; Siegmund, A.; Boezio, A. A.; Booker, S.; Choquette, D.; D'Angelo, N. D.; Germain, J.; Yang, K.; Yang, Y.; Zhang, Y.; Bellon, S. F.; Whittington, D. A.; Harmange, J.-C.; Dominguez, C.; Kim, T.-S.; Dussault, I. Structure-based design of novel class II c-Met inhibitors: 2. SAR and kinase selectivity profiles of the pyrazolone series. *J. Med. Chem.* **2012**, *55*, 1868–1897.

(17) Bodendorf, K.; Mildner, J.; Lehman, T. Antipyrinealdehyde and antipyrinic acid. *Justus Liebigs Ann. Chem.* **1949**, *563*, 1–11.

(18) Shaw, G.; Sugowdz, G. Isoxazolinones. VI. The hydrogenation of 5-amino-isoxazoles. A new synthesis of pyrimidines. *J. Chem. Soc.* **1954**, 665–668.

(19) Engelhardt, H.; Boehmelt, G.; Kofink, C.; Kuhn, D.; McConnell, D.; Stadtmueller, H. Preparation of pyrimidinonecarboxylic acid amides with antiproliferative activity. WO2010007114A2, 2010.

(20) Ishiyama, T.; Murata, M.; Miyaura, N. Palladium(0)-catalyzed cross-coupling reaction of alkoxydiboron with haloarenes: a direct procedure for arylboronic esters. *J. Org. Chem.* **1995**, *60*, 7508–7510.

(21) Doxycycline-induced overexpression of PERK in HT1080 cells transfected with the T-REX-PERK-FLAG construct results in significant PERK autophosphorylation. Therefore, no external UPR activator (such as thapsigargin) is required in this cell line for activation of PERK in the assays described.

(22) Kolb, H. C.; Sharpless, K. B. The growing impact of click chemistry on drug discovery. *Drug Discovery Today* **2003**, *8*, 1128–1137.

(23) Carnahan, J.; Beltran, P. J.; Babij, C.; Le, Q.; Rose, M. J.; Vonderfecht, S.; Kim, J. L.; Smith, A. L.; Nagapudi, K.; Broome, M. A.; Fernando, M.; Kha, H.; Belmontes, B.; Radinsky, R.; Kendall, R.; Burgess, T. L. Selective and potent Raf inhibitors paradoxically stimulate normal cell proliferation and tumor growth. *Mol. Cancer Ther.* **2010**, *9*, 2399–2410.

(24) Nagar, B.; Bornmann, W. G.; Pellicena, P.; Schindler, T.; Veach, D. R.; Miller, W. T.; Clarkson, B.; Kuriyan, J. Crystal structures of the

kinase domain of c-Abl in complex with the small molecule inhibitors PD173955 and imatinib (STI-571). *Cancer Res.* **2002**, *62*, 4236–4243.

(25) Steiner, T. Water molecules which apparently accept no hydrogen bonds are systematically involved in C–H...O interactions. *Acta Crystallogr., Sect. D: Biol. Crystallogr.* **1995**, *51*, 93–97.

(26) We were unable to obtain cocrystal structures of our compounds with GCN2, but the structure of apo yeast GCN2 is known. This made comparison of apo GCN2 (PDB accession code 1ZYC) with apo PERK (PDB accession code 3QD2) the most appropriate.

(27) Cui, W.; Li, J.; Ron, D.; Sha, B. The structure of the PERK kinase domain suggests the mechanism for its activation. *Acta Crystallogr., Sect. D: Biol. Crystallogr.* **2011**, *67*, 423–428.

(28) Padyana, A. K.; Qiu, H.; Roll-Mecak, A.; Hinnebusch, A. G.; Burley, S. K. Structural basis for autoinhibition and mutational activation of eukaryotic initiation factor 2 α protein kinase GCN2. *J. Biol. Chem.* **2005**, *280*, 29289–29299.

(29) Still, W. C.; Kahn, M.; Mitra, A. Rapid chromatographic technique for preparative separations with moderate resolution. *J. Org. Chem.* **1978**, *43*, 2923–2925.

(30) D'Angelo, N. D.; Kim, T.-S.; Andrews, K.; Booker, S. K.; Caenepeel, S.; Chen, K.; Freeman, D.; Jiang, J.; McCarter, J. D.; San Miguel, T.; Mullady, E. L.; Schrag, M.; Subramanian, R.; Tang, J.; Wahl, R. C.; Wang, L.; Whittington, D. A.; Wu, T.; Xi, N.; Xu, Y.; Yakowec, P.; Zalameda, L. P.; Zhang, N.; Hughes, P.; Norman, M. H. Discovery and optimization of a series of benzothiazole phosphoinositide 3-kinase (PI3K)/mammalian target of rapamycin (mTOR) dual inhibitors. *J. Med. Chem.* **2011**, *54*, 1789–1811.

(31) *QuantiGene 2.0 Reagent System. User Manual*; Panomics, Inc.: Santa Clara, CA, 2007; http://www.panomics.com/downloads/UM13074_QG2Manual_RevB_080102.pdf.